7-2020

Environmental Influences on Tree-driven Karst Bedrock Physical Weathering

Cole Robert Jimerson
University of Arkansas, Fayetteville

Environmental Influences on Tree-driven Karst Bedrock Physical Weathering

A thesis submitted in partial fulfillment
of the requirements for the degree of
Master of Science in Geology

by

Cole Robert Jimerson
College of Wooster
Bachelor of Arts in Geology, 2014

July 2020
University of Arkansas

This thesis is approved for recommendation to the Graduate Council.

Jill A. Marshall, Ph.D.
Thesis Director

Matthew Covington, Ph.D.
Committee Member

Kusum Naithani, Ph.D.
Committee Member

Abstract

The role of tree roots as stressors that contribute to physical weathering processes and thus soil generation remains an open question in critical zone science. While evidence suggests roots may be able to damage rock by accessing pre-existing fractures, where they can expand due to water uptake or generate forces on rock in response to wind gusts, these processes have not been investigated in temperate karst regions until now. I monitored forces at the root-rock interface for an American elm and Hackberry tree between September 2019 and May 2020. I used piezoelectric force sensors to determine if differences in species, tree size, the distance of roots from the tree, wind or precipitation conditions affected the frequency or magnitude of forces exerted by tree roots onto bedrock. I analyzed meteorological conditions in addition to root forces to examine the environmental controls on diurnal cycles of forces exerted on the bedrock and to identify how roots responded to wind gusts and rainfall events. Roots of both species exerted higher daily forces between the hours of 10:30 and 23:00, reaching daily maximum forces between 15:00 and 18:00, and exerting forces for approximately an extra hour during the fall and spring compared to the winter. I determined that temperature's impact on vapor pressure deficit, which controls the rate of transpiration, was the primary driver of the timing of daily forces. Precipitation led to periods of higher forces, as the roots expanded due to water-uptake as well as reduced tree transpiration from lower VPD and solar radiation during rainfall events. Roots of greater size exerted increasing fluctuations in forces onto the bedrock in response to wind gusts and rainfall. American elm roots exerted forces on the bedrock more frequently during windy periods compared to the Hackberry roots. Variations in the root response to wind and precipitation events are hypothesized to be linked to contrasting rooting strategies between species and the specific functional role of individual roots in supporting the tree. My findings suggest that in warmer conditions, with more intense rainfall events, roots will exert greater forces on bedrock due to 1) increased temperature-controlled vapor pressure

deficit and, 2) heavy rainfall-induced forces due to water uptake. These projected increase in forces suggest that in the karst landscape of Northwest Arkansas, tree roots may accelerate the physical weathering of bedrock.

Acknowledgements

This study could not have been accomplished without the guidance and help of Dr. Jill Marshall and my committee members. I would like to thank Dr. Van Brahana for detailed hydrological information of Savoy Experimental Watershed, along with Josh Blackstock, Cooper McCabe, and Sam Zapp for their help with data analysis. Funding for this study was provided by start-up funds from Dr. Jill Marshall and the University of Arkansas and the Geological Society of America graduate research grant. Finally, I would like to thank Ben Kumpf from the University of Victoria for help assisting me with some of the Python coding conducted throughout this study.

Table of Contents

List of Figures

LIST OF TABLES

1. Introduction

Soil is one of the most vital materials on Earth, supporting and providing nutrients for crops, wetlands, and forests which we depend on for food, fuel, and raw materials; storing, filtering, and transporting rainwater; offering habitats for wildlife, domestic livestock, and micro-organisms; and supplies the foundation and building materials for man-made infrastructure (Harrison et al., 2011). As issues regarding climate change persist, soil will prove to be an important resource that mitigates the impacts of extreme weather events, helps regulate Earth's temperature, and stores large amounts of CO_2 and other greenhouse gasses (Harrison et al., 2011). Understanding the interconnected processes on the Earth's surface and subsurface and their role in generating soil, sculpting the landscape, and building the foundation for terrestrial ecosystems is the primary goal of research within the "critical zone" – the near-surface layer that spans from the vegetation canopy to the solid unweathered bedrock below, where water, rock, and life meet and interact (Riebe et al., 2017). This permeable layer of Earth's surface contains weathered rock (regolith) that is weathered and eroded in the subsurface, allowing it to become broken up into mobile material that is transported across the landscape as sediment (Riebe et al., 2017; Anderson, 2019).

The physical damaging or weathering of rock is the initial step in detaching rock so that it can be converted into soil. This is accomplished by increasing the available surface area for reactions to occur and creating smaller particles that can be moved more easily, which promotes both chemical weathering and erosion (Anderson, 2019). However, our understanding of chemical weathering is much more comprehensive than that of physical weathering processes, especially in temperate landscapes where most of our understanding is conceptual. Physical weathering is generated as a result of stresses that damage the rock such as thermal expansion (Eppes et al., 2016), frost cracking (Rempel et al., 2016), mineral volumetric expansion (Goodfellow et al., 2016), and root growth (Pawlik et al., 2016). Through these processes, the properties of the rock such as strength, porosity, and hydraulic conductivity are

altered which directly affect the rate of mobile sediment production and hence the potential of rock being able to be detached into soil (Anderson, 2019).

Rock is most often observed on the surface of the Earth breaking critically through destructive failure events, such as tree-throw and landslides, yet these are rare and often episodic, and research suggests subcritical forces also damage rock in many environments (e.g. Eppes and Keanini, 2017). The physical breakdown of rock stems from the propagation of cracks within the rock. These cracks propagate or grow once the “critical’ stress is reached that exceeds the strength of the rock, which is controlled by material properties such as tensile strength or fracture toughness (Eppes and Keanini, 2017). However, cracks also grow slowly and steadily over time – subcritically – from stress much lower than the critical stress of the rock (Atkinson, 1984; Eppes and Keanini, 2017). These subcritical stress conditions are likely to occur in all surface and near-surface rocks over long-term periods (10^1 – 10^6 years), during which these small stresses decrease the force needed to break the rock as the crack length grows (Eppes et al., 2016; Eppes and Keanini, 2017). Furthermore, subcritical stresses are additive, meaning that all these stresses accumulate together adding to the total stress exerted on the rock (Eppes and Keanini, 2017). Thus, over geologic time scales exceeding 10^1 – 10^6 years, small forces can exceed the strength of the rock, causing it to crack sub-critically and will damage the rock (Eppes and Keanini, 2017).

Current research has begun to identify the role that tree roots play below ground in the critical zone, yet many limitations still exist. The roots of trees can anchor the plant to the underlying substrate providing support as well as transporting essential nutrients and water in addition to aiding in biochemical processes key to their survival (Anderson 2019). While most research has explored how trees play a role in soil transport, removal, and stabilization acting as a source of soil cohesion (Dietrich and Perron, 2006; Gabet and Mudd, 2010; Pawlik et al., 2016; Brantley et al., 2017), it remains unknown if roots have the ability to actually break rocks as a result of limited data availability (Anderson, 2019). Studies on the role of roots within

bedrock have found that although roots cannot physically penetrate solid bedrock, in environments with thin to no soil, they can access pre-existing fractures to access the bedrock at depths ranging from centimeters to many meters below ground (Zwieniecki and Newton, 1994; Matthes-Sears and Larson, 1995; Hasenmueller et al., 2017). While previous work has observed root density, growth, and depth of trees growing into rock (Matthes-Sears and Larson, 1995; Schwinning, 2008, 2013; Estrada-Medina et al., 2013; Ni et al., 2015; Phillips, 2016), all of these investigations fail to address the role of roots in physically applying forces onto the rock and propagating cracks further (Anderson, 2019).

While some studies suggest roots can exert radial pressures of 0.51 – 0.9 MPa from root growth (Misra et al., 1986) and thus infer the ability of roots to widen joints within the rock (Pawlik et al., 2016), current research measuring the forces that trees exert on rock suggests that root growth pressures likely do not play a significant if any role on the rate of forces acting on rocks (Marshall, 2018). Marshall (2018) has identified that root forces exerted on rock is likely caused by water-uptake induced root swelling and wind-driven root movement acting on the rock. While water-uptake driven root forces are likely not sufficient enough to exceed the tensile strength of the rock, they can exert smaller forces on the rock and as suggested by Atkinson (1987), stresses on the rock as low as one-tenth of the tensile strength can lead to subcritical cracking. Additionally, during rarer windstorms, root forces caused by wind-driven movement may be able to exceed the tensile strength of rocks (Marshall, 2018). These findings imply that over the lifetime of an individual tree, which can be decades to centuries, subcritical forces exerted by tree roots via environmental stresses can lead to rock damage or fracturing.

Trees absorb water through their root tips within the soil or surrounding bedrock (Meyer et al., 1973). Water is then transported from these root tips upwards through the roots, up the stem, and ultimately to the leaves through xylem ducts, the principal water-conducting tissue of the plant (Meyer et al., 1973). Diurnal variations in tree root and stem diameter are of regular occurrence, reaching minimum diameter when the water columns are under maximum tension,

becoming stiff and decreasing in diameter (Meyer et al., 1973). As a result of strong adhesion between water and the xylem duct walls, slight contractions occur in their diameter (Meyer et al., 1973). Thus, the diurnal variations in tree diameter are from the alternate contraction of the vessels or tracheid's when water is under tension, followed by dilation when the tension is relaxed which is controlled by replenishment and dehydration of the trees water storage (Meyer et al., 1973; Turcotte et al., 2011). "As a general rule, stem and roots contract in the daytime, when the transpiration and photosynthesis processes are vigorous, and expand at night when water reserves are gradually replenished" (Turcotte et al., 2011).

For tree roots growing into fractures or wedged against bedrock, these daily changes in pressure on the bounding rock wall have the potential to induce subcritical stresses on the enfolding rock over the lifetime of the tree (Marshall, 2018). Transpiration of trees is controlled primarily by solar radiation, humidity, and temperature (Meyer et al., 1973). Solar radiation is the primary driver as transpiration cannot occur without the presence of sunlight, while humidity controls the rate of transpiration with greater vapor pressures leading to slower transpiration rates (Meyer et al., 1973). Furthermore, rises in temperature lead to an increase in the steepness of the vapor gradient through the stomate of the leaves, hence increasing transpiration (Meyer et al., 1973). Throughout the day, while transpiration is occurring rapidly, the rate of absorption of water cannot keep pace with the rate of water vapor loss from the leaves (Meyer et al., 1973). This results in an overall reduction of the water content within the entire plant during mid-daylight, before peak transpiration (Meyer et al., 1973).

During the nighttime, water continues to move upwards after transpiration has ceased due to the residual negative water potentials of the leaf cells (Meyer et al., 1973). Water can also move both laterally in roots and the stem as well as downward from the leaves to the trunk, from areas of positive to negative water potential (Meyer et al., 1973). The rate of water absorption within the tree typically lags the rate of transpiration during daylight hours, with peak absorption rates occurring later in the day than peak transpiration rates (Meyer et al., 1973).

During the night, the rate of absorption is continuously higher than transpiration, however, these absorption rates are lower than the normal daytime rate (Meyer et al., 1973).

In response to wind gusts, tree roots can exert forces on the surrounding bedrock as the tree sways, which will be further referred to as wind-driven root movement (Marshall, 2018). Trees rooted in thin, stony soils can experience root movement as high as 60 mm during large wind gusts imposing forces on the rock at the root-bedrock interface (Rizzo and Harrington, 1988). Preliminary work at Critical Zone Observatories in California, North Carolina, and Colorado, measuring root-bedrock forces has provided insights on how tree sizes, species, and properties control the magnitude and frequency of forces that roots exert on the enfolding rock (Marshall, 2018). Tree sway is primarily controlled by tree properties including mass, elasticity, wood density, and canopy structure (Moore and Maguire, 2004). Furthermore, tall, wide trees will respond differently than small, thin trees, and similarly, trees with differing crown architecture will respond differently to wind gusts (van Emmerik et al., 2017). Tree properties such as elasticity, stiffness, mass, and canopy structure influence each tree's response to wind gusts, hence, dictating the frequency and magnitude of wind-driven tree movement which exerts forces on roots embedded in surrounding rock.

Progress on characterizing the ability of tree roots to physically weather bedrock and quantifying soil production mechanisms is limited by a lack of direct measurements of the forces exerted by trees. Marshall (2018) used force-sensors to measure the forces exerted by tree roots on the underlying bedrock along with precipitation, solar radiation, wind speed, and tree sway movement from accelerometers to determine the mechanisms that influence tree-driven bedrock physical weathering. In the absence of tree-throw, forces generated by roots that result from the trees swaying in response to wind gusts and root swelling as the trees take up water in response to rainfall and daily transpiration cycles are the dominant mechanisms by which trees can damage bedrock over the lifetime of the tree (Marshall, 2018). Furthermore, many questions remain, such as how the timing and the amount of rainfall influence the forces that are

exerted on the bedrock in response to water-uptake, as well as how individual tree species may respond differently. These driving questions and missing links in our understanding of exactly how trees can physically weather bedrock has led to the motivation for this study in the temperate karst landscape in Northwest Arkansas (Fig. 1).

1.1 Hypotheses

H1) Tree-driven forces exerted on the bedrock will increase throughout the night as water-uptake exceeds transpiration, increasing the diameter of roots and applying pressure to the surrounding bedrock. During daylight hours, tree-driven forces on the bedrock will decrease as transpiration exceeds water-uptake, causing the tree roots to shrink in response to water stress.

H2) Tree-driven forces exerted on the surrounding bedrock will increase and remain greater following rainfall events as the roots swell due to additional water-uptake.

H3) Larger trees will respond less frequently to wind gusts, exerting forces at a lower frequency onto the surrounding bedrock. On the other hand, slender trees will respond more frequently to wind gusts, exerting forces more often, at a higher frequency on the bedrock.

H4) Tree roots further away from the tree will require large, persistent wind events to exert forces on the bedrock in response to wind-driven tree movement, as only very large wind events are expected to impart enough energy to induce root forces at far distances from the tree trunk.

2. Study Design

In this study, two trees were continuously monitored at a site in a watershed of mixed-species, temperate deciduous trees over eight months from September 2, 2019, through May 2, 2020. To test the four hypothesizes above, I installed force sensors on roots of an *Ulmus americana* (American elm) and *Celtis occidentalis* (hackberry) tree that have varying heights,

diameters at breast height (DBH), estimated stem mass, root diameter, and distance from the tree (Table 1). In addition, I measured environmental conditions including precipitation, short-wave radiation, wind speeds, and temperatures.

Table 1. Measured roots of this study along with their root characteristics, tree species, measured sizes, and wood properties.

Root ID	Root Diameter (cm)	Distance from tree (cm)	Tree Species	Tree Height (m)	Tree DBH (cm)	Stem Mass (kg)	Wood Density (g/cm^3)	Modulus of elasticity
CH-1	7	40	Hackberry	28.2	51.6	5774.5	0.49	0.95
CH-7	6	400	Hackberry	28.2	51.6	5774.5	0.49	0.95
CH-4	7	77	American Elm	12.9	34.7	1122.6	0.46	1.11
CH-5	10	120	American Elm	12.9	34.7	1122.6	0.46	1.11

2.1 Site Description

The Savoy Experimental Watershed (SEW) in Savoy, Arkansas is located in the mantled karst of the Springfield Plateau in the southwestern Ozark Plateaus (Fig. 1). This region has a temperate climate, characterized by mean annual temperatures of ~ 14°C, with the monthly mean temperature being the highest in July (~ 26°C) and lowest in January (~ 2°C), mean annual precipitation of ~ 117 cm/year, with the wettest month being May (~ 13.6 cm) (PRISM Climate Group, 2020). SEW is divided into six sub-watersheds with Basin-1 being the focus of most of the past research, being well-characterized and well-instrumented and is the focus of the current investigation (Fig. 1). While Basin-1 is underdrained by Langle and Copperhead Springs which form an underflow/overflow system (Brahana et al., 1999; Pennington, 2010), Copperhead Spring is where the trees in this study were monitored (Fig. 1, 2, 3). Copperhead Spring is the overflow conduit in the system, which experiences lower discharge rates and drains a much smaller portion of the drainage area of the watershed during low-flow conditions (Brahana et al., 1999; Pennington, 2010). However, during high-flow conditions, Copperhead has a more rapid and larger flow reaching up to 0.75 m^3/s (Brahana et al., 1999; Pennington, 2010).

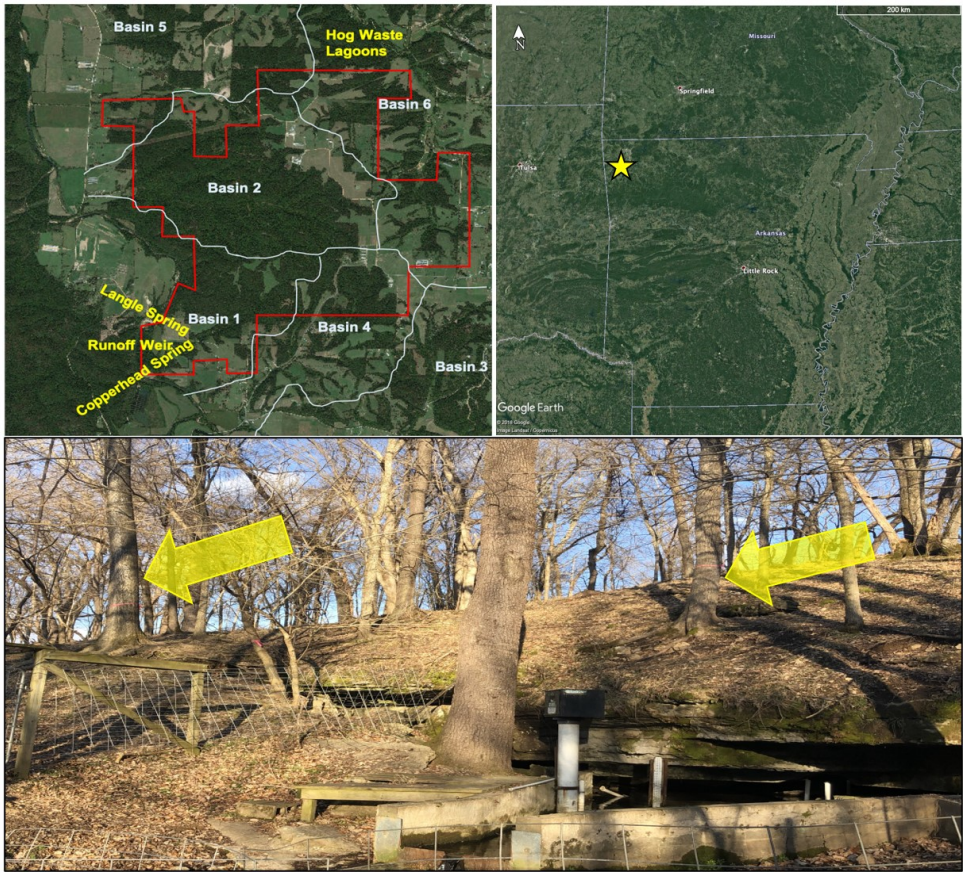

Figure 1. Copperhead Spring field site (bottom) with the two trees being studied (marked with yellow arrows). The location of Copperhead Spring within SEW (top left) and the location of SEW in Arkansas marked with a star (top right) (Photo by Author).

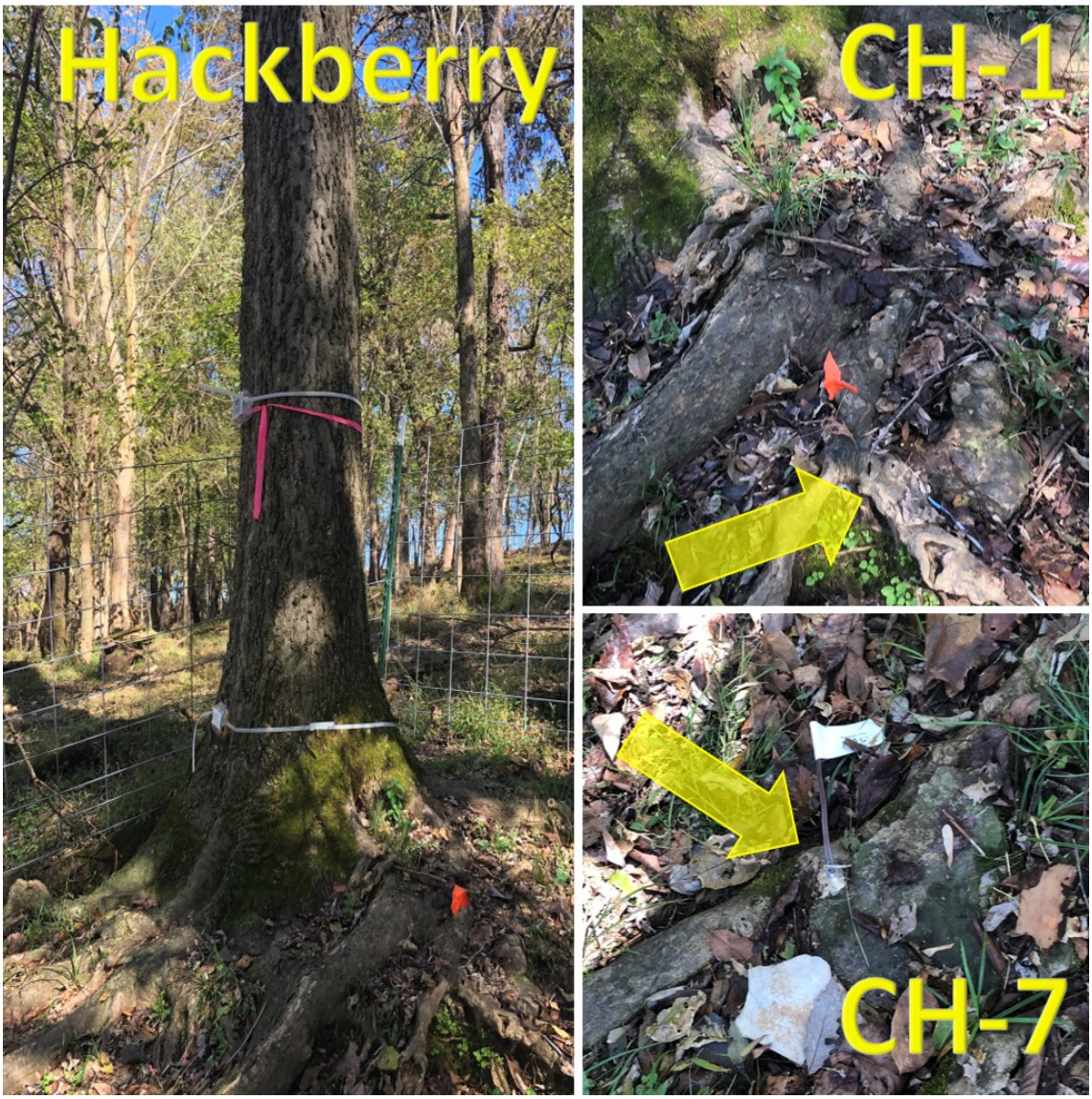

Figure 2. Hackberry tree at Copperhead Spring and the two roots that were instrumented (indicated with yellow arrows) with force sensors at the root-rock interface (Photo by Author).

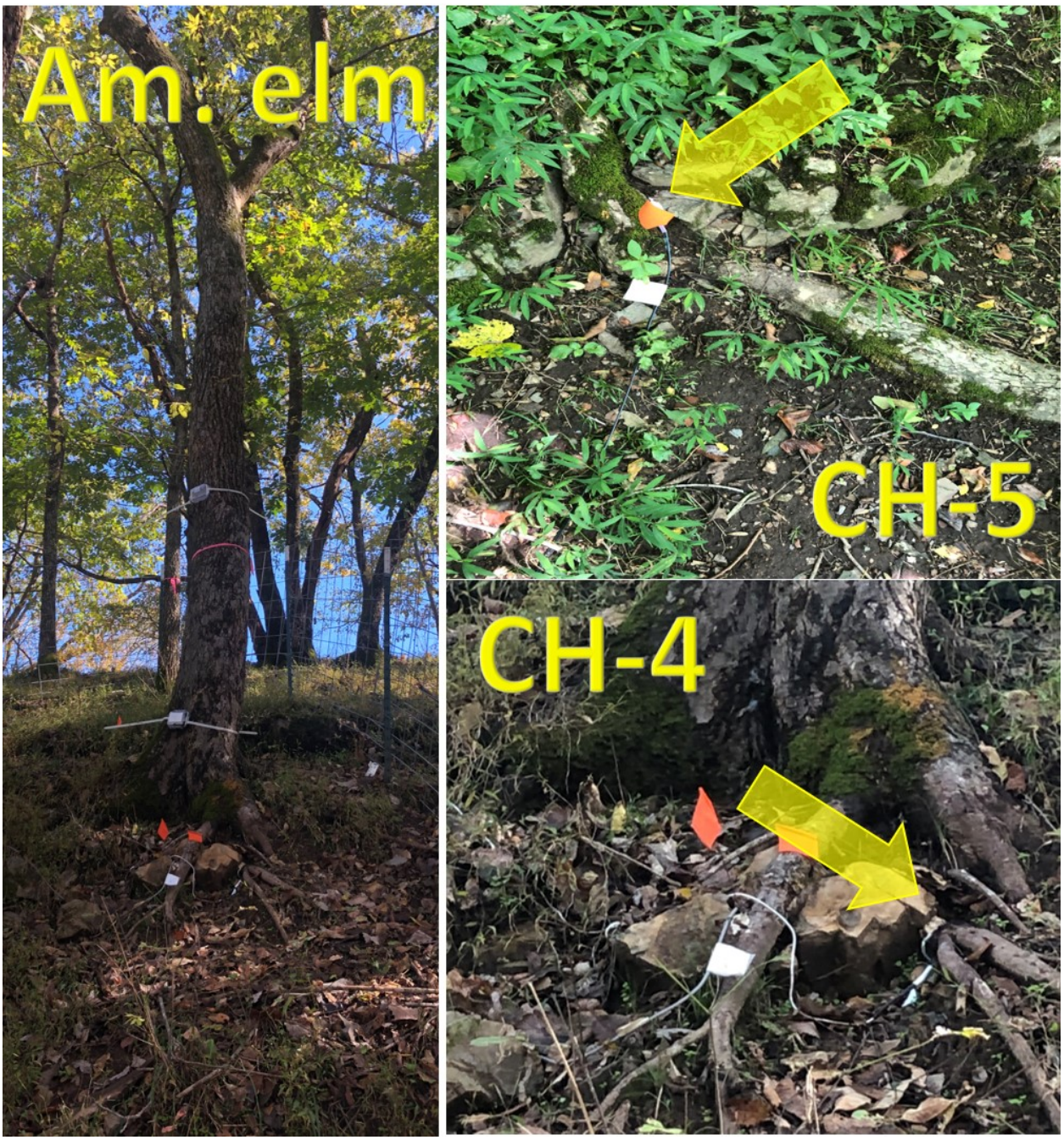

Figure 3. American elm tree at Copperhead Spring and the two roots that were instrumented (indicated with yellow arrows) with force sensors at the root-rock interface (Photo by Author).

2.2 Methods

To quantify root forces on bedrock, I instrumented roots growing into or wedged between bedrock fractures at Copperhead Spring (Fig. 2, 3) with FlexiForce piezoelectric force sensors (Fig. 4). I measured the average forces exerted by trees onto bedrock over ten-minute intervals from September 2 – November 24, 2019. I then increased the sampling frequency to collect the average force over one-minute intervals on November 24, 2019 – May 2, 2020. These sensors are small (25.4mm long by 14mm wide and only 0.203mm thick), permitting them to be inserted between the tree-bedrock interface (Fig. 4), to collect measurements of forces exerted from tree roots directly onto the enfolding rock. All the force sensors in this study are attached to multi-channel Campbell CR1000X dataloggers.

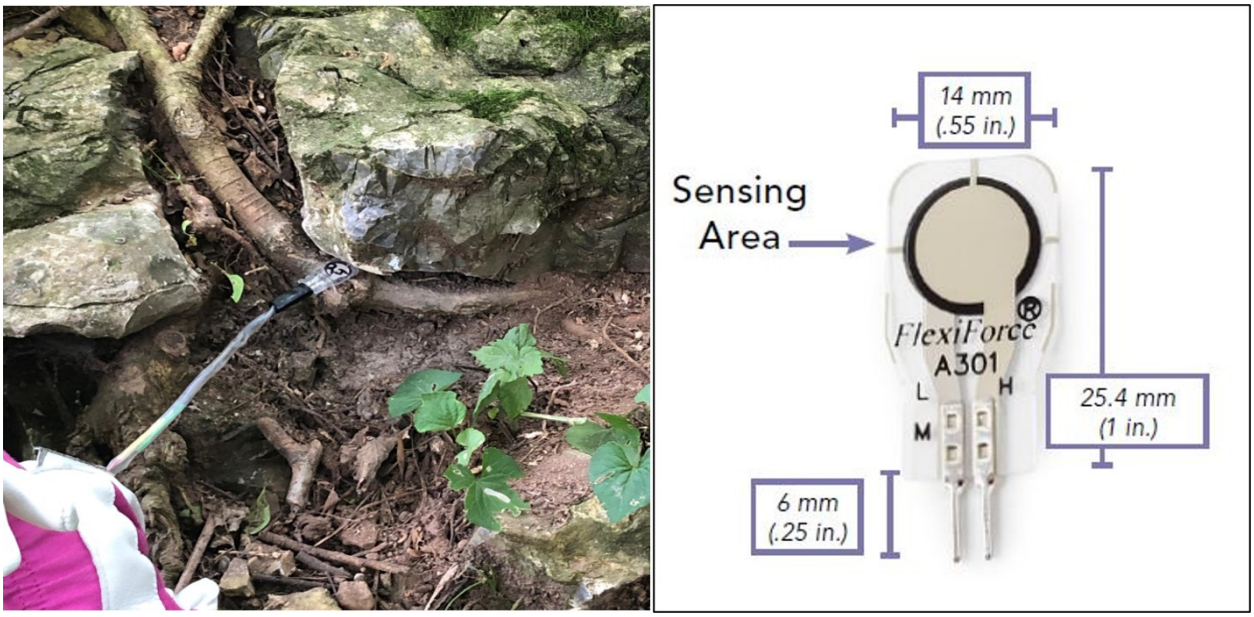

Figure 4. (Left) Example of a FlexiForce piezoelectric force sensor being installed at the root-rock interface and (Right) sensor dimensions (Photo by Author).

The FlexiForce sensors output resistance values that I converted into a voltage which can then be output by the datalogger using a half-bridge with a 3000 ohms resistor. I collected electrical output measurements as the ratio of voltage $_{in}$ / voltage $_{out}$ from the datalogger and converted the values back into resistance values in ohms using the equation:

$$R_s = R_f \frac{X}{1 - X}$$

where R_s is the resistance of the sensors (ohms), R_f is the feedback resistance of the resistor (3000 ohms), and X is the sensor output (voltage $_{out}$ / voltage $_{in}$). Prior to deployment in the field, I created a force-resistance calibration curve (Fig. 5) for each sensor by measuring the outputted resistance from the sensor as force. I applied loads in increments ranging from 0.013 – 4.4 kN using a load cell attached to a Universal Testing Machine (UTM). This allowed for an estimate of the amount of force at the root-rock interface, using the resistance values outputted by the sensors. Since these sensors are not meant to handle both static and dynamic loads occurring over different time intervals, it was not possible to predict the combination of loads such that I cannot accurately predict the drift of the sensors and calibrate the sensors accordingly in the lab. As a result, I used changes in resistance values as a proxy for changes in forces over time, as the actual force values of the sensors under field conditions do not match the calibrated values developed using a single type of load over time intervals of a few seconds in the lab. However, the outputted resistance values over short time scales still provide qualitative information about the magnitude of forces experienced at the root-rock interface.

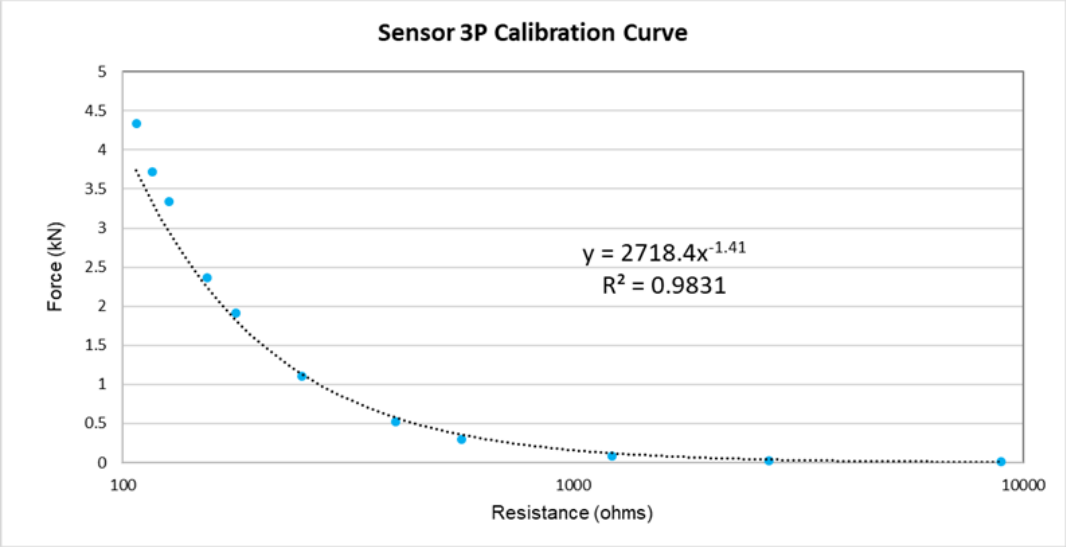

Figure 5. Example of an existing calibration curve for a force sensor installed on a root of an American Elm tree at Copperhead Spring.

To test the hypothesis (H3) that trees of different species, size, and tree properties will respond differently to wind gusts, I used a HOBO Wind Speed Smart Sensor (S-WSB-M003) to measure average wind speed and highest three-second gust speed over five minutes intervals from September 2 – November 24, 2019. I then increased the recording period to one-minute intervals after November 24, 2019, for better resolution, at the weather station located upstream of Copperhead Spring. I measured diameter at breast height (DBH) using a standard measuring tape and tree height (h) using a laser range finder. Wood properties of density (ρ_w) and the modulus of elasticity were taken from Green et al. (1999) and Chave et al. (2009). Wood density is often negatively related to the ability of wood to store and release water under tension (Chave et al., 2009). This suggests that trees with higher densities may take up less water, possibly exerting less force on the rock associated with mass changes from water uptake. The mass of the tree stem for each tree was estimated using a standard equation of a cylinder. Although these calculations do not include the tree crown, they can be used as indicative measurements to compare and explain the results from different trees. I used each of these tree properties to

help explain variations in wind-driven tree-forces that are measured with the force sensors at the root-bedrock interface.

In addition, I recorded precipitation, solar radiation, humidity, and temperature measurements at five minutes intervals from September 2 – November 24, 2019, and one-minute intervals after November 24, 2019, at the weather station. Measurements of solar (short-wave) radiation were used to correlate with resistance values at the root-rock interface to discern daily variations in root forces associated with root-water uptake from changes in tree transpiration. Precipitation measurements were also correlated with resistance values at the root-rock interface to link fluctuations in root forces that result from increased water uptake during rainfall events (Marshall, 2018). Vapor pressure deficit (VPD) was calculated using the temperature and relative humidity data. VPD is the difference between the air-water content and the maximum amount of water the air can carry at a given temperature.

To determine if discharge at the nearby Copperhead spring was influencing the forces exerted by the roots onto the bedrock, primarily in terms of water uptake, discharge measurements were collected at the spring using weirs and submersible pressure transducers (Fig. 6) by Abby Rhodes, a researcher at the University of Arkansas. Discharge from the spring was used as a proxy for subsurface water flowing to each site throughout the investigation. Discharge measurements from the spring were used to identify flow patterns, rather than precise values, to determine how much water may be available from the subsurface or nearby stream for roots to uptake.

Figure 6. Weir installed at Copperhead Spring at SEW that was used to measure spring flow discharge along with Abby Rhodes who collected the measurements (Photo by Author).

2.3 Sensor Temperature Sensitivity and Drift

The output of the FlexiForce sensors, used to measure forces at the root-rock interface, can vary up to approximately 0.36% per change in degree Celsius (Appendix 1.2) from the initial temperature at which the sensor was calibrated in the lab (~ 21°C). This temperature sensitivity causes the output force readings to be higher (lower resistance) as temperature increase above 21°C and output lower forces (higher resistance) the more temperatures decrease below 21°C (Fig. 7). To account for the effect of temperature sensitivity (± 0.36% per °C) I took the most conservative assumption (that temperature sensitivity was at its maximum) and corrected my resistance data using the equation:

$$R_T = R_S + (R_S \times (0.36\% \times (T_I - T_F)))$$

where R_T is the corrected resistance for temperature sensitivity, R_S is the output resistance of the sensor, T_F is the average temperature in the field, and T_I is the initial temperature when the sensor was calibrated.

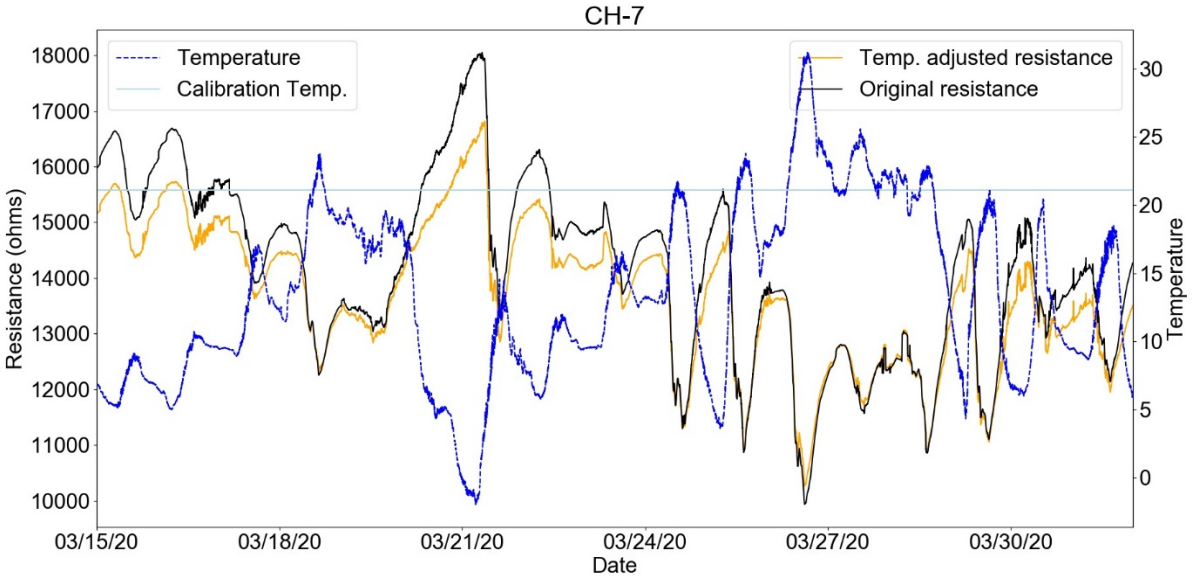

Figure 7. Adjusted resistance values (orange) compared to the original output resistance values (black), as temperature (blue) varies above and below the temperature at which the sensor was calibrated (light blue). In this example, the derived force value variation is very low as the resistance values recorded here are an order of magnitude higher than the lowest calibrated resistance for this sensor.

The FlexiForce sensors, like all piezoelectric sensors drift, or change sensor output over a period of time, when a constant force is applied. The sensor drift causes the output resistance of the sensor to continually decrease (forces appear to increase) at a rate of < 5% per logarithmic time – with 'time' being determined by the expected time period over which a static load is applied (Appendix 1.2). Sensors are normally calibrated to account for this drift by applying loads at the known time scale at which loads will be applied in the field. However, in this study, the sensors are subject to static loads over multiple timescales that were previously

unknown before the completion of this study. For example, forces due to root swelling may increase over one-hour time periods (a dynamic load), but are generally steady over ten-minute time periods, while root forces may remain fixed over daytime or nighttime intervals due to cyclic water uptake and transpiration. However, these values are not easily segmented, given multiple drivers such as solar radiation, VPD, and temperature. Similarly, wind-driven root forces increase or decrease over the time scale of seconds. To correct for this, I have created an uncertainty bound of a 5% drift per several logarithmic time to determine the range of possible resistance values that could be possible, using the equation:

$$R_D = R_T + (R_T \times (5\% \times (log10(time\ since\ deployment))))$$

where R_D is the maximum boundary for possible resistance values when corrected for drift, R_T is the corrected resistance for temperature sensitivity, and the time since deployment is in both minutes and seconds. The uncertainty boundary of resistance values accounting for drift was calculated in both minutes and seconds (time since deployment). Calculating drift using seconds time scale would plot the greatest possible drift as time increases every second, while the minutes time scale is the same as the sampling interval and is a more likely case for the experienced drift.

2.4 Data Analysis

I used Python (version 3.7.4), a programming language, for all analyses described below. I calculated the first derivative of all data points for each force sensor in the time-series to observe the change in forces over time in response to wind gusts. The derivative of forces in this study is defined as:

$$\frac{\Delta y}{\Delta x} = \frac{y_2 - y_1}{x_2 - x_1}$$

where y is resistance (ohms) and x is time (minutes) between each adjoining data point in the time-series. Then I normalized the derivative values of force to obtain values between 0 and 1.

The normalized derivatives of each force sensor were filtered for when wind gusts exceed 4 m/s, to identify how the forces were changing during periods of higher wind gust speeds. The value of 4 m/s was selected as the cutoff value for wind gusts as significant fluctuations tended to occur during winds of this speed. To qualitatively determine if the trees were responding to the wind gusts, I plotted the masked derivate values along with the full data set of derivate values along with the wind speeds, rainfall events, and temperature. This provides the opportunity to both compare the amount and time of changes in forces during higher wind speeds to times when no wind speeds were occurring as well as being able to determine if rainfall or temperature changes were occurring during these periods.

I resampled rainfall to a one-hour total rainfall to identify large rainfall events. This displays if many rainfall events occurred within the hour (i.e. high rainfall intensity) or just a single rainfall event (i.e. low rainfall intensity). To determine if there was any correlation between root forces and rainfall events, I masked the entire dataset for when any rainfall occurred. This created a separate dataset with only the force values when rainfall occurred, which was plotted on top of the original force values, showing the exact moment when rainfall happened.

To separate daytime and nighttime rainfall events, I masked the dataset when shortwave radiation was less than 1 W/m^2 (no solar radiation) and when shortwave radiation was greater than 1 W/m^2 (solar radiation). This separation of values, easily identified how values were changing during the day and at night and discerned how the diurnal variation of forces is shifting as solar radiation increases and decreases throughout each 24-hour cycle. By combining all three of these methods above, I determined visually how many times it rained throughout any given period, the times when rainfall was more intense, and whether it was occurring during the day or night.

To determine the timing of diurnal variations in root forces on the bedrock as well as environmental conditions including shortwave radiation, temperature, humidity, and vapor pressure deficit, I separated the entire dataset for every minute of the day and parsed into a single dataset for each minute of every day of the time-series. I then calculated the mean and standard deviation for each group of values occurring at each minute of the day, forming a 1440-minute daily trend. For each month of this study, the daily trend was observed for the whole time-series of that month. Then to identify seasonal changes, I grouped months based on average Normalized Difference Vegetation Index value groups with fall containing September, October, and November; winter containing December, January, February; and spring consisting of March and April. This allows for the analysis of how the forces changed throughout a typical day of the month compared to environmental variables that tend to exhibit daily fluctuations as well. By analyzing from month to month and by season, seasonal changes in forces can be observed that occur from the fall before the leaves drop, in the winter when there are no leaves on the trees and the trees are overall less active, and in the spring as the trees begin to bloom and become more active.

All correlations between weather variables and root forces were conducted using the PAST statistical software (Hammer et al. 2010). To determine the general correlation between all the variables in the dataset and the changes throughout the study period, I calculated Pearson's r using all variables (excluding rainfall) for each month of the study (Appendix 3.1). Furthermore, I computed multivariate linear regressions using the force values as the dependent variables and the weather values as the independent variables. The multivariate linear regression identifies more directly (using all the variables) which weather variables are best correlated with each root force.

3. Results

3.1 Environmental Variables and Root Forces

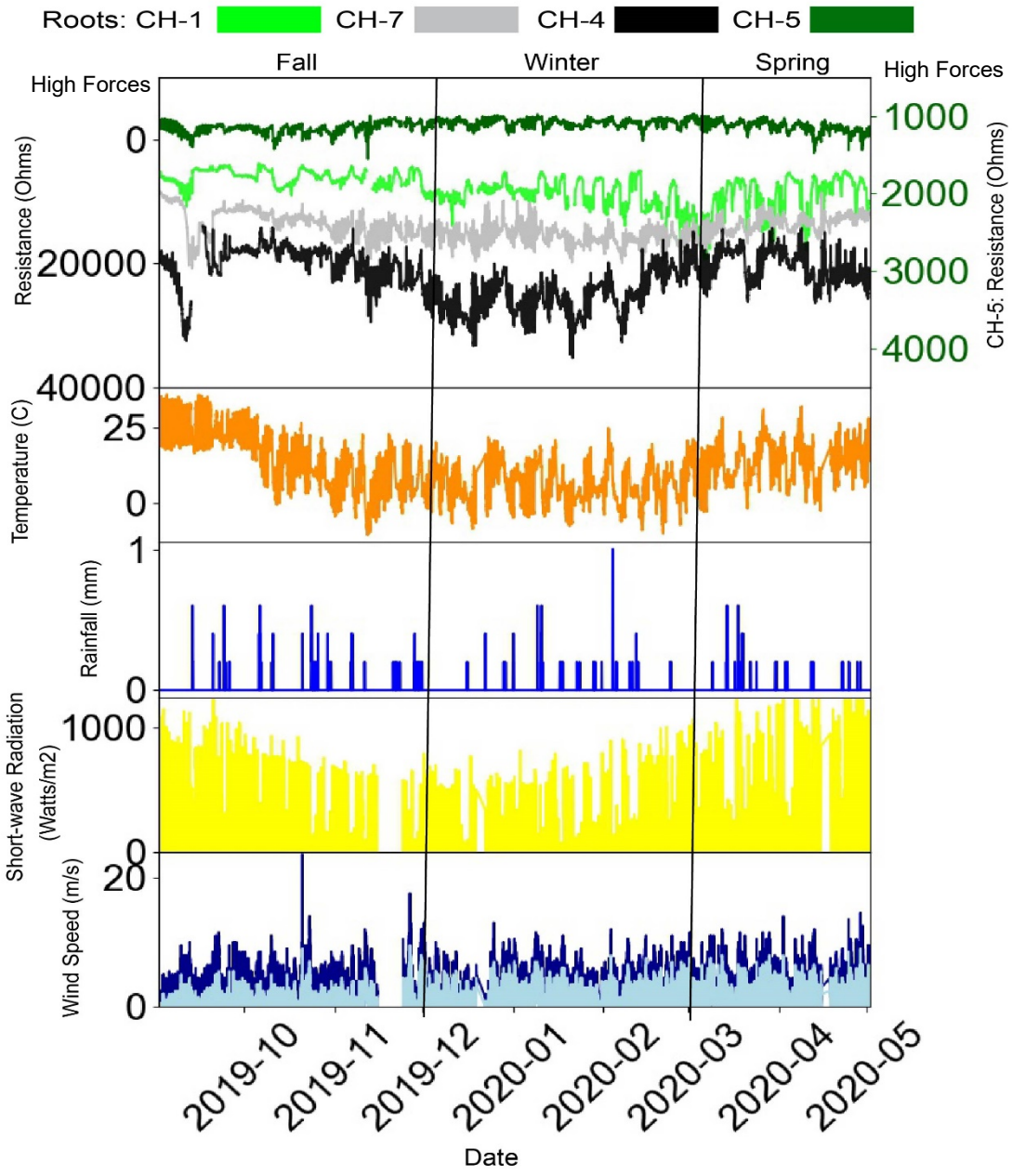

Figure 8. Time-series of root forces represented as resistance (ohms) for all four roots in the study and meteorological data collected from September 2, 2019 – May 2, 2020. Root CH-5 (dark green) is plotted on the right y-axis as the resistance values vary an order of magnitude from the other sensors on the rest of the roots in this study. Wind speed is plotted as average wind speed (light blue) and gust speed (dark blue). Gaps in the plot are due to periods with no data due to memory errors in the equipment.

Throughout the study period of September 2, 2019, through May 2, 2020, the highest amount of precipitation and days of heavy rainfall occurred during the fall season, specifically during October where 58 rainfall events were recorded (equivalent to 11.6 mm of rainfall) over nine days (Fig. 8). May was the second wettest month with 37 rainfall events (7.4 mm of rainfall), with most of the rainfall occurring within five heavy rainfall days. January was the driest month, experiencing only 7 rainfall events (1.4 mm of rainfall) on five separate days. Wind and gust speeds were typically between 1 m/s and 2 m/s respectively, with gust speeds reaching as high as 23.7 m/s in the fall and 17.6 m/s in the spring. However, wind gusts throughout the study tended to only reach speeds of 10 – 12 m/s during windy days. The dominant wind direction was S/SSW for all months except for April where wind directions shifted to be dominantly WNW. Temperature and relative humidity tended to occur in an inverse fashion, where temperature increased while relative humidity decreased during the day and flipped during the nighttime (Fig. 9). Similarly, when large drops in temperature occurred, large increases in relative humidity occurred at the same time, which tended to occur before rainfall events (Fig. 9). Temperature was most strongly correlated with the far Hackberry root (CH-7) and the large American elm root (CH-5) and showed slightly weaker correlations with the smaller American elm root (CH-4), but no correlation was observed with the close Hackberry root (CH-1) (Appendix 3).

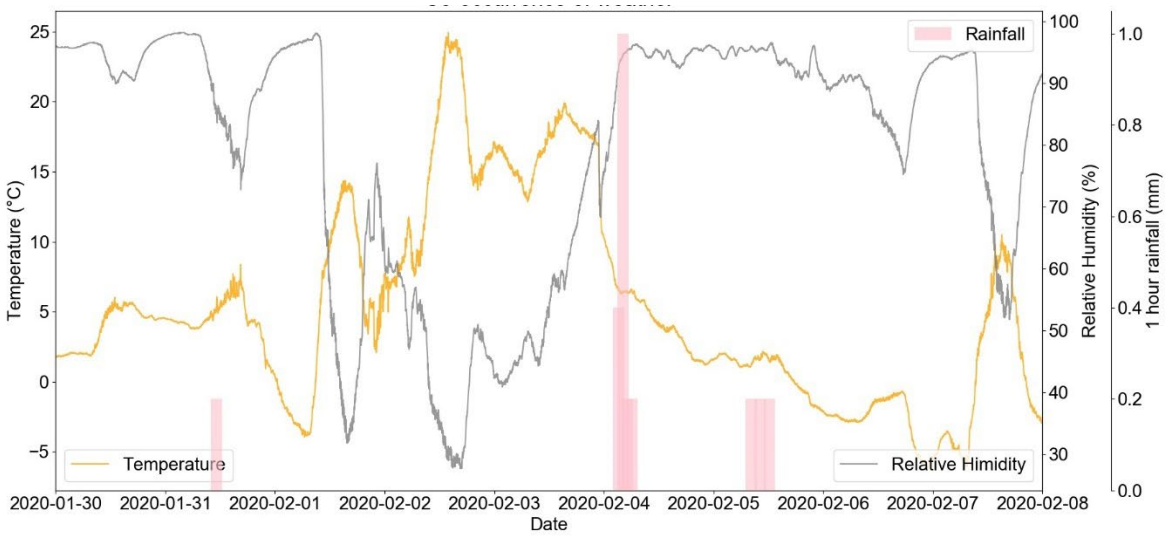

Figure 9. Temperature (orange), relative humidity (grey), and rainfall (pink bars) occurring from January 30 – February 8, 2020. Temperature increases as relative humidity decreases and during rainfall event a large increase in relative humidity occurs as temperature sharply decreases.

3.2 Timing of Root Forces

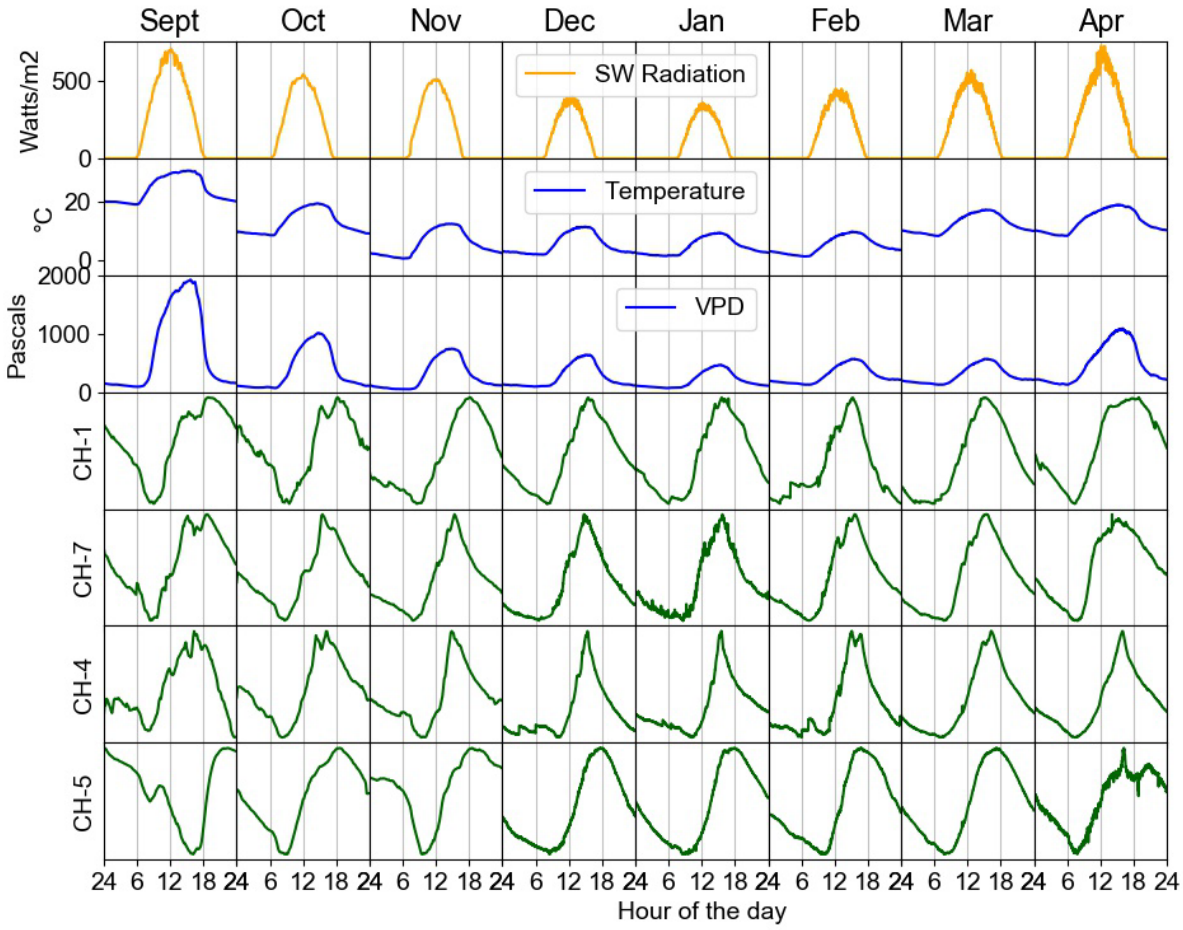

Figure 10. Monthly mean diurnal cycle for shortwave radiation, temperature, vapor pressure deficit, and root forces for all four roots during each month of the study period. Daily variations in root forces are plotted to only show the change in average values, the change in amplitude is not shown.

Peak forces for all roots typically occurred between the hours of 15:00 – 19:00. Peak shortwave radiation occurred between 12:00 – 13:00, while both peak temperature and VPD occurred between 14:00 – 16:00. The peak minimum forces (T_{min}) tended to vary more between roots, tending to take place between 7:00 – 10:00. However, peak minimum daily temperature and VPD occurred between 5:30 – 7:30 (Fig. 10).

Table 2. Descriptive statistics of the monthly mean diurnal cycles presented in Fig. 9. The hour of the day that the average daily maximum (T_{max}) and minimum (T_{min}) force occurred for each root with their respective range in resistance values (amplitude) and associated standard deviation.

Month	Root ID	T_{max} (hour of day)	T_{min} (hour of day)	Amplitude (ohms)	± STDV
September	CH-1	19	9	509	521
	CH-7	19	9	825	758
	CH-4	16	24	1246	544
	CH-5	0	16	79	20
October	CH-1	18	10	239	829
	CH-7	16	9	1048	175
	CH-4	16	8	1417	482
	CH-5	19	9	80	6
November	CH-1	18	9	745	1665
	CH-7	15	8	3061	128
	CH-4	15	9	3131	111
	CH-5	19	10	75	4
December	CH-1	15	8	1152	514
	CH-7	15	7	2559	126
	CH-4	15	10	3502	276
	CH-5	18	8	67	10
January	CH-1	16	6	987	717
	CH-7	16	9	1819	70
	CH-4	16	10	3058	618
	CH-5	18	9	55	2
February	CH-1	15	2	1656	987
	CH-7	16	7	2237	176
	CH-4	15	6	2296	100
	CH-5	17	10	58	11
March	CH-1	15	6	2495	1717
	CH-7	15	8	2089	7
	CH-4	16	7	2994	374
	CH-5	17	8	82	8
April	CH-1	19	7	1549	1190
	CH-7	14	8	1300	191
	CH-4	16	7	3790	502
	CH-5	16	8	52	2

Table 3. The hour of the day that the average daily maximum (T_{max}) and minimum (T_{min}) shortwave radiation, temperature, and vapor pressure deficit occurred and with their respective values and standard deviation.

Month	Variable	T_{max} (hour of day)	T_{min} (hour of day)	Max value	± STDV	Min value	± STDV
September	SW Radiation (W/m2)	12	n/a	700	295	-	-
	Temperature (C°)	15	6	31	4	19	2
	VPD (Pa)	16	6	1927	907	94	94
October	SW Radiation (W/m2)	12	n/a	540	265	-	-
	Temperature (C°)	15	7	20	7	9	6
	VPD (Pa)	15	7	1014	650	72	64
November	SW Radiation (W/m2)	12	n/a	510	236	-	-
	Temperature (C°)	14	6	13	7	1	7
	VPD (Pa)	15	7	744	461	52	44
December	SW Radiation (W/m2)	13	n/a	400	207	-	-
	Temperature (C°)	15	7	12	6	2	6
	VPD (Pa)	16	6	640	420	96	79
January	SW Radiation (W/m2)	12	n/a	360	230	-	-
	Temperature (C°)	15	6	10	6	2	6
	VPD (Pa)	15	6	470	375	71	75
February	SW Radiation (W/m2)	13	n/a	450	286	-	-
	Temperature (C°)	15	7	10	6	1	6
	VPD (Pa)	15	7	571	489	129	167
March	SW Radiation (W/m2)	13	n/a	570	290	-	-
	Temperature (C°)	15	7	17	6	8	7
	VPD (Pa)	15	7	571	620	129	135
April	SW Radiation (W/m2)	12	n/a	720	388	-	-
	Temperature (C°)	16	6	19	6	9	5
	VPD (Pa)	16	6	1090	698	130	142

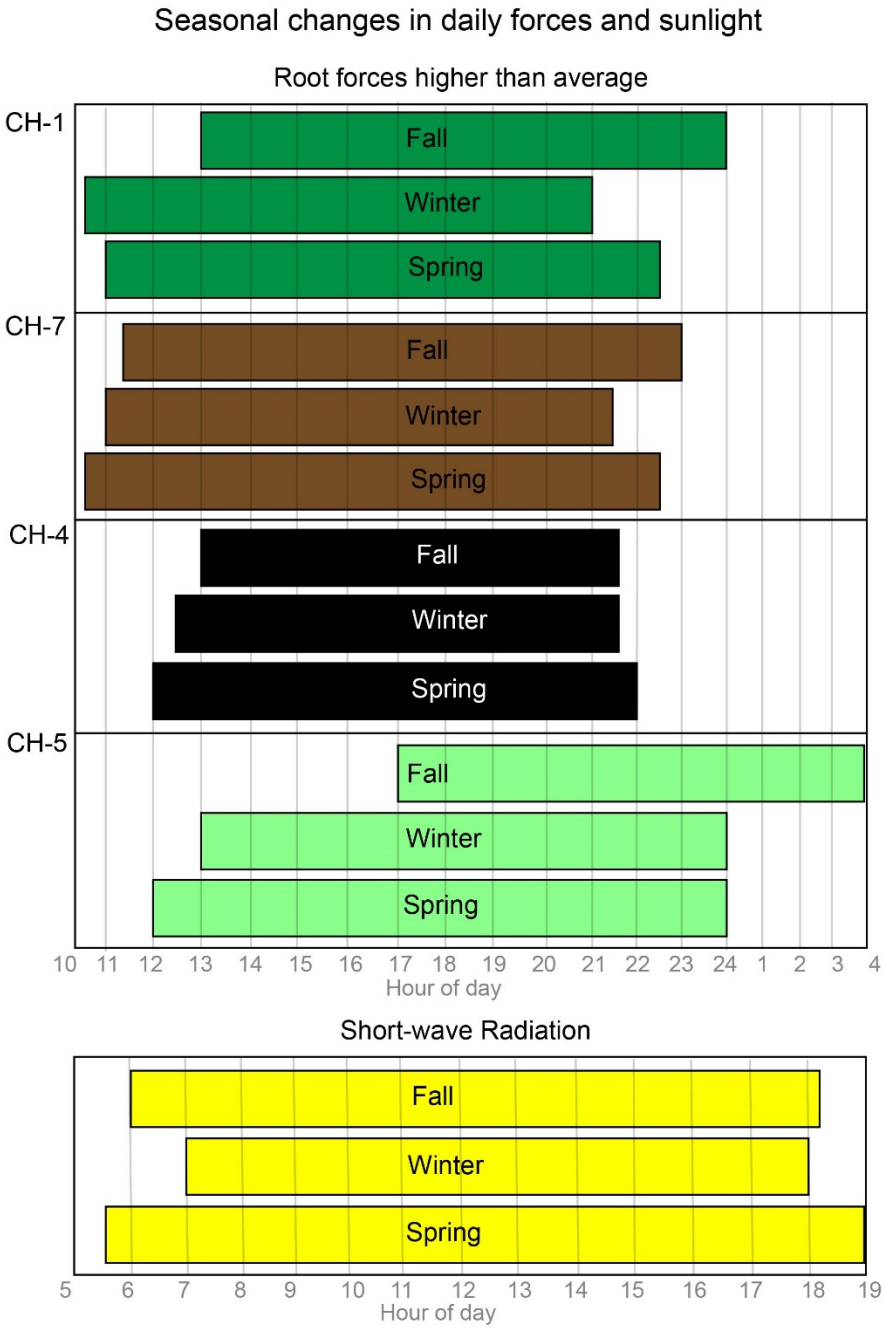

Figure 11. The length of time that the root forces exerted onto the bedrock was higher than the average throughout the daily cycle for each season and the length of time that solar radiation is active during each season (yellow). The bars represent the beginning and end of the time during the day (in hours on the x-axis) that the roots exert forces onto the bedrock during each season.

The roots of the Hackberry tree (CH-1 and CH-7) showed similar trends in their timing of forces on the bedrock. Both roots exhibited higher than average forces typically between 10:30 - 23:00 throughout the study period. Furthermore, there was a shift in the amount of time the roots exerted higher forces on the bedrock as the seasons change. Forces were exerted for a longer period throughout the day in the fall (11 hours) and spring (11.5 hours) compared to the winter (10.5 hours) for each root (Fig. 11). The Hackberry roots also exerted higher daily forces on the bedrock later into the night during the fall and spring months compared to the winter (Fig. 11).

The roots of the American Elm tree (CH-4 and CH-5) exhibited slightly different timing of forces throughout the day. The larger root (CH-5) exhibited higher than average forces for approximately 11 hours during the fall and winter, and the longest amount of time in the spring (12 hours), similar to the Hackberry roots (Fig. 11). The small root (CH-4) exerted forces on the bedrock for the shortest amount of time during the fall (8.5 hours), increasing into the winter (9 hours) and spring (10 hours). The American Elm roots shifted their timing of higher forces throughout the study, beginning earlier in the day as the seasons' transition from fall to winter into spring (Fig. 11). Also, the large root exerted the longest period of higher forces on the bedrock during the day (11 – 12 hours) compared to any other root in the study, while the small root exhibited the shortest period of increased forces on the bedrock during the day (8.5 – 10 hours).

Daily averages of solar radiation also changed throughout the study period as the seasons changed. During the fall months, there was a relatively long period of solar radiation (6:00 – 18:00) and higher amounts (>800 W/m2). In the winter months, solar radiation is both the shortest (7:00 – 18:00) and the lowest (~600 W/m2). Similarly, to the forces, we see the longest period of shortwave radiation during the spring months (5:30 – 19:00) as well as the highest average daily values (~1000 W/m2).

3.3 Wind-induced Root Forces on Rock

The root of the Hackberry tree that was monitored closest to the trunk (CH-1) rarely responded to wind gusts, displaying fluctuations in forces typically only when wind gusts exceeded 6 m/s, and with forces increasing as the gust speeds increased. This root also displayed occasional large increasing fluctuations in force when gust speeds exceed 8 m/s (Fig. 12). Also, larger wind gusts tended to occur during rainfall events, which led to large increases in forces and even wind gusts as low as 5 m/s led to minor fluctuations in forces during the rainfall events even though the general trend of the forces was constant and high. The smaller Hackberry root monitored ~4 meters from the tree (CH-7), responded differently with the highest fluctuations in forces occurring during the day when wind gusts between 4 – 6 m/s were sustained for many hours (Fig. 12). Fluctuations in forces were the highest during constant wind gusts, where forces fluctuated more frequently and at a higher rate of change than CH-1 (Fig. 12).

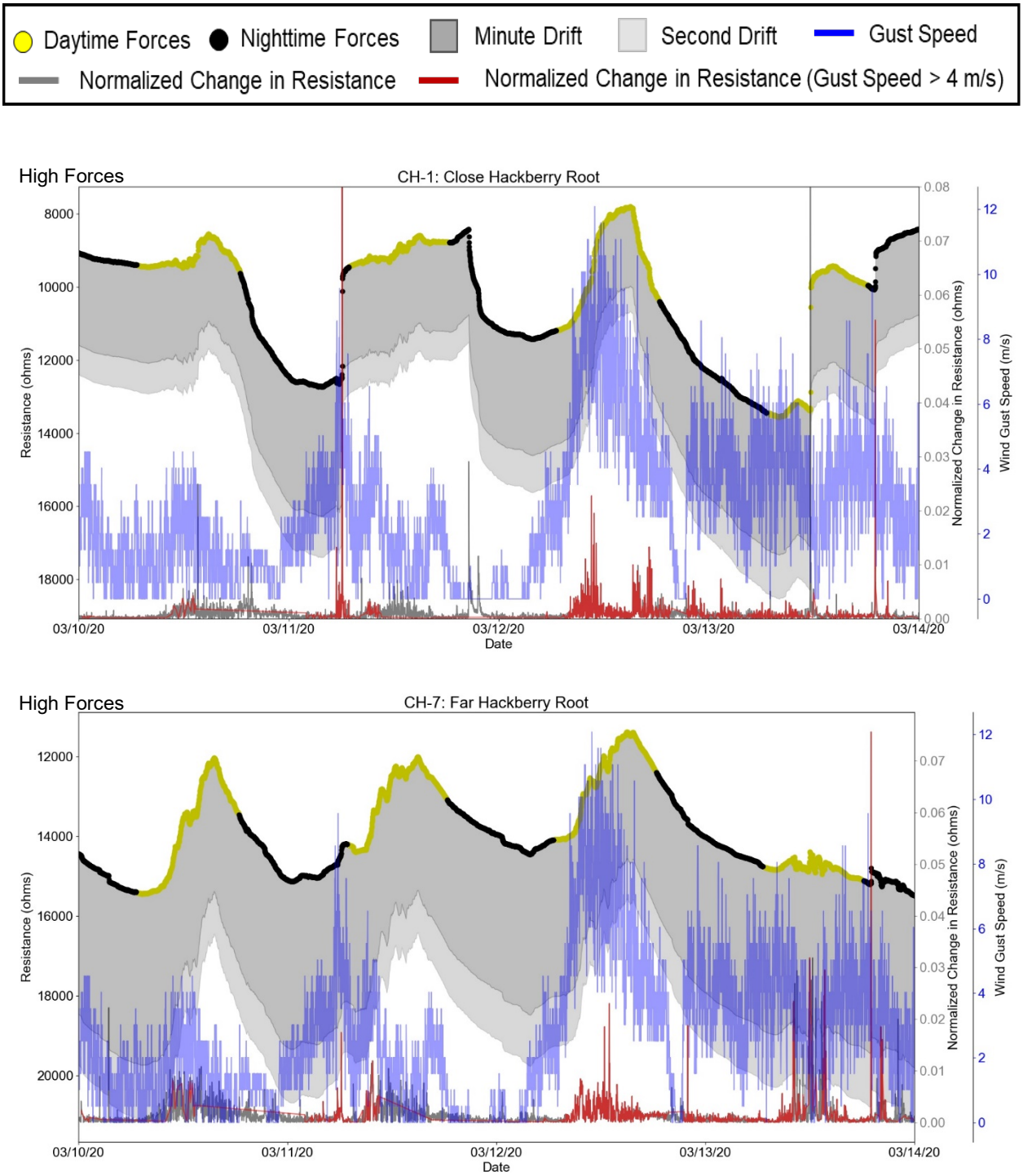

Figure 12. Hackberry tree roots (CH-1 and CH-7) forces and normalized change in forces (grey/red) during low, high, and sustained wind gust speeds. Force derivates in root forces are in grey when wind gusts are less than 4 m/s and when wind gusts exceeded 4 m/s are indicated in red. The yellow line indicates forces when solar radiation is active and black when it is absent. The grey region indicates the uncertainties in the possible range of calibrated force-resistance curve values due to sensor drift under static loads over one-second (light grey) and one-minute (dark grey) log intervals.

The large root of the American elm tree (CH-5), showed the greatest response to wind events throughout the study period. This larger root exhibited minor fluctuations in forces in response to all wind gusts that exceeded 4 m/s and continued fluctuating at a much higher rate as wind gusts remained sustained for many hours or days. Larger fluctuations in forces arose when wind gusts exceeded 6 m/s or when hours of consistent wind gusts exceeding 6 m/s occurred, which caused much higher fluctuations (Fig. 13). Following rain events, although the forces decreased in general, many fluctuations of forces in response to wind gusts even at 4 m/s occurred more often and larger than the typical fluctuations during non-rain days.

The smaller American elm root (CH-4) below the tree required higher sustained gust speeds (typically exceeding 6 m/s) for the root to induce larger fluctuations in forces on the bedrock (Fig. 13). The fluctuations in forces on the bedrock became bigger when sustained wind gusts exceeded 10 m/s during the night or when sustained wind gusts exceeded 6 m/s for many hours after rain events ensued. However, CH-4 responded similarly to the Hackberry roots, with much lower changes in forces during windy days compared to CH-5 (Fig. 13). The co-occurrence of larger fluctuations in forces during no wind or rain days during the day time when roots normally exerted higher forces on the bedrock and the occurrence of intermediate winds made it difficult to determine the direct cause of these fluctuations (Fig. 13).

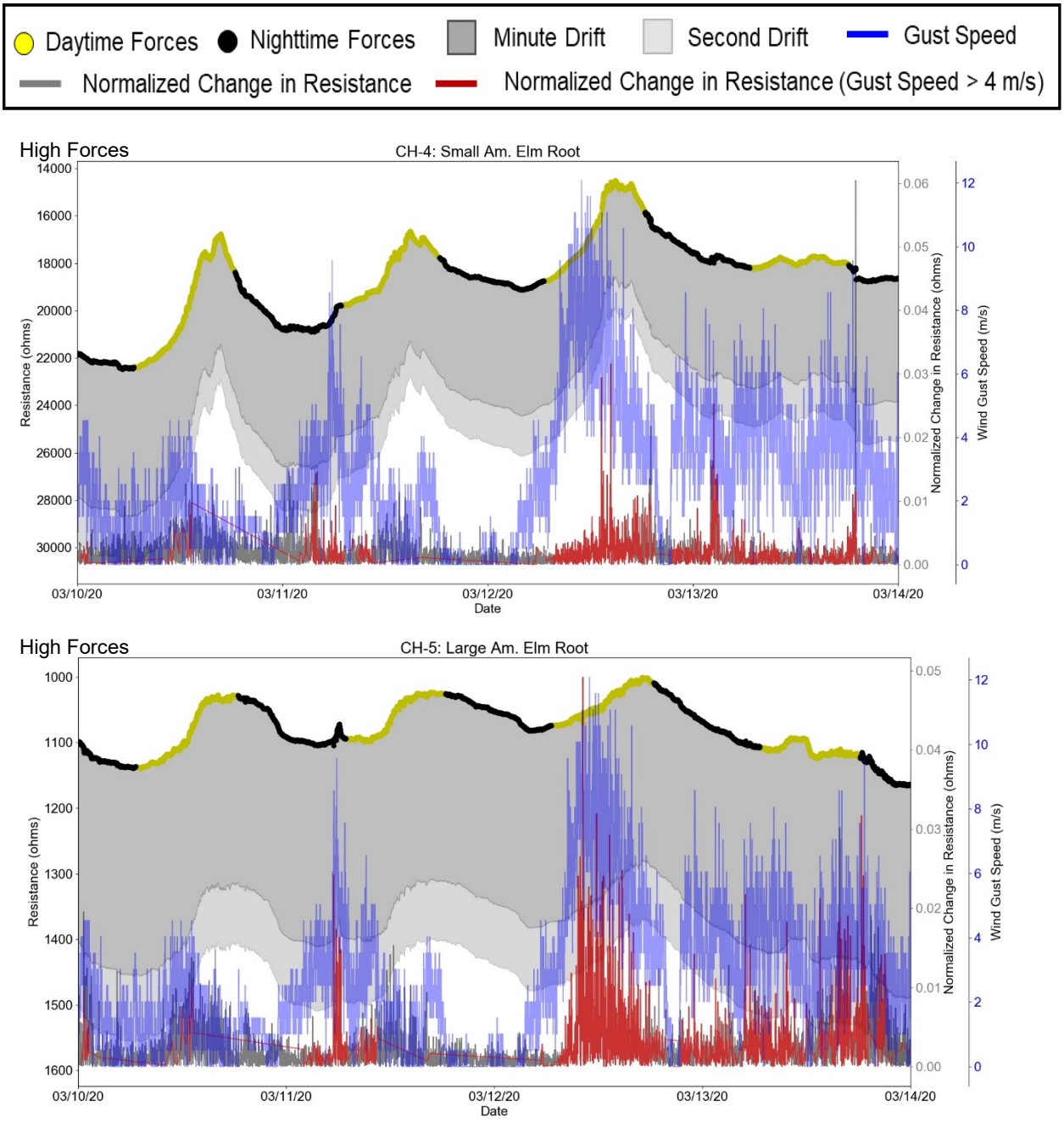

Figure 13. American elm roots (CH-4 and CH-5) forces and normalized change in forces (grey/red) during low, high, and sustained wind gust speeds. Force derivates in root forces are in grey when wind gusts are less than 4 m/s and when wind gusts exceeded 4 m/s are indicated in red. The yellow line indicates forces when solar radiation is active and black when it is absent. The grey region indicates the uncertainties in the possible range of calibrated force-resistance curve values due to sensor drift under static loads over one-second (light grey) and one-minute (dark grey) log intervals.

3.4 Root-water Uptake

The root of the Hackberry tree that was monitored 0.3 m from the trunk (CH-1), responded much differently than the other three roots. Following any rainfall event, forces increased and remained much higher than normal, remaining higher anywhere from 12 hours to a full day (Fig. 14). This trend of continued higher forces was amplified when multiple rainfall events occurred in the following hours or days, remaining much higher until at least half a day transpired, then forces began to drop as it transitioned into the afternoon. The root of the American elm tree that was monitored 0.5 m below the tree (CH-4) responded similarly to the root of the Hackberry tree that was monitored 4 m from the tree (CH-7) during rainfall events. Both roots displayed increases in force following each rainfall event both during the day or at night. Yet these roots were much less affected and increases in forces were either much smaller or did not occur in response to rainfall events that followed the initial rainfall event. These roots showed their largest increase in forces when individual rainfall events were more than an hour apart, rather than continuous rainfall events. On the other hand, the American elm tree root that was the largest of the study (~ 13 cm in diameter) (CH-5) showed a much different response. This root displayed slight increases following heavy rainfalls or continuous rainfall events. However, the overall daily trend of forces exerted by this root was not greatly affected by rainfall, specifically individual rainfall events. Surprisingly, this root occasionally exhibited decreases in forces in response to rain events (Fig. 15).

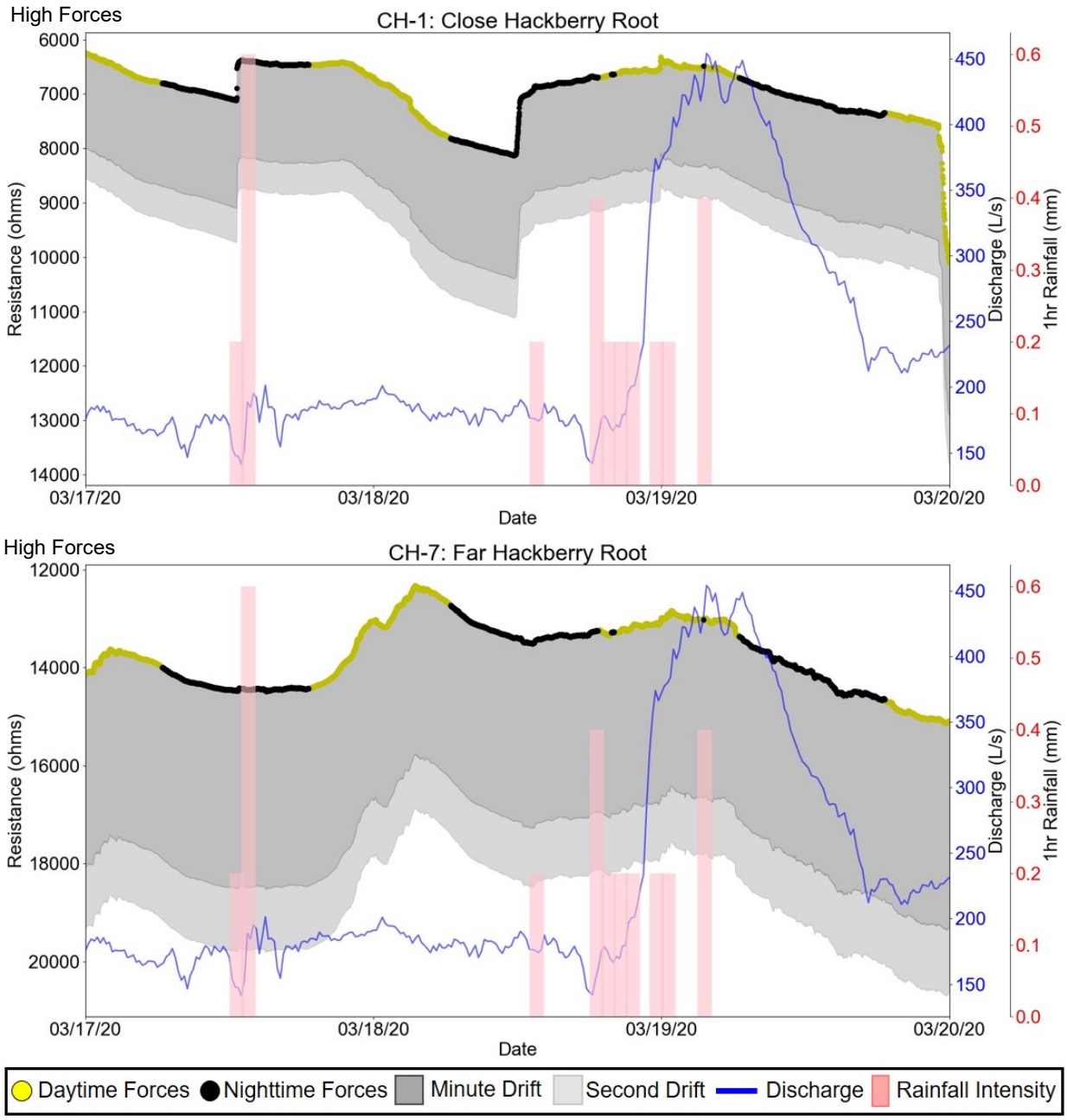

Figure 14. Changes in root forces on the bedrock for the Hackberry roots (CH-1 and CH-7) over three days that experienced heavy rainfall followed by a large increase in discharge. The yellow line indicates forces when solar radiation is active and black when it is absent. The grey region indicates the uncertainties in the possible range of calibrated force-resistance curve values due to sensor drift under static loads over one-second (light grey) and one-minute (dark grey) log intervals.

During September and October, both CH-1 and CH-4 showed large increases in forces during rainfall events. The more rainfall that occurred during the rainfall event, the larger the increase in forces, then forces dropped back down afterward. CH-7 also displayed a generally similar trend but smaller increases in response to rain events, while CH-5 shows initial slight increases in forces when it rained, then a larger decrease in forces immediately after rainfall events.

During January, CH-1 showed a much different response with forces being higher during rainfall events and remaining constantly higher as it continued to rain, even when there were multiple hours separating rainfall events, with forces decreasing many hours after the last rainfall (Fig. 14). Forces additionally remain much higher and only increase very slightly when there was a full day of no rainfall in between rainfall events. Forces tended to increase largely before the rainfall occurred, which coincided with both large temperature changes and large wind gusts, then show an increasing trend as it continued to rain but then stayed constant. Forces began to rise again and remain constant after it rained the next day. As it transitioned towards the spring months, longer times were required for the forces to return to the normal daily trend and typically stayed higher for multiple days following the rainfall events. If it rained every one to two days, the forces remained higher overall and there was not much change from day to night, staying relatively constant compared to the normal daily trend. Forces continued to overall increase as more intense rainfall occurred, yet forces tended to only increase very slightly by individual rainfall events during this time unless they occurred on separate days (i.e. we see an increase when it rained again a day later after the previous rainfall event) (Fig. 14).

CH-7 exhibited a different response to rainfall than CH-1, with the daily variation in forces being diminished when it rained, and forces remained relatively constant. Forces began to drop a few hours after the last rainfall and the diurnal trend resumed the next day. Even when it rained two days later, the diurnal variation in forces still was lessened, returning to normal a

few hours after the last rain event. Forces tended to increase after it rained and the nighttime drop in forces became either much less than normal or stayed relatively constant throughout the night. Forces increased in response to rainfall events, even if the overall trend was still decreasing, both during the day and night (Fig. 14). When it rained during the day, an increase in forces occurred followed by a decrease, while rainfall into the night typically caused increases but not always. However, when it only rained at night, forces remained constant following the rainfall (Fig. 14).

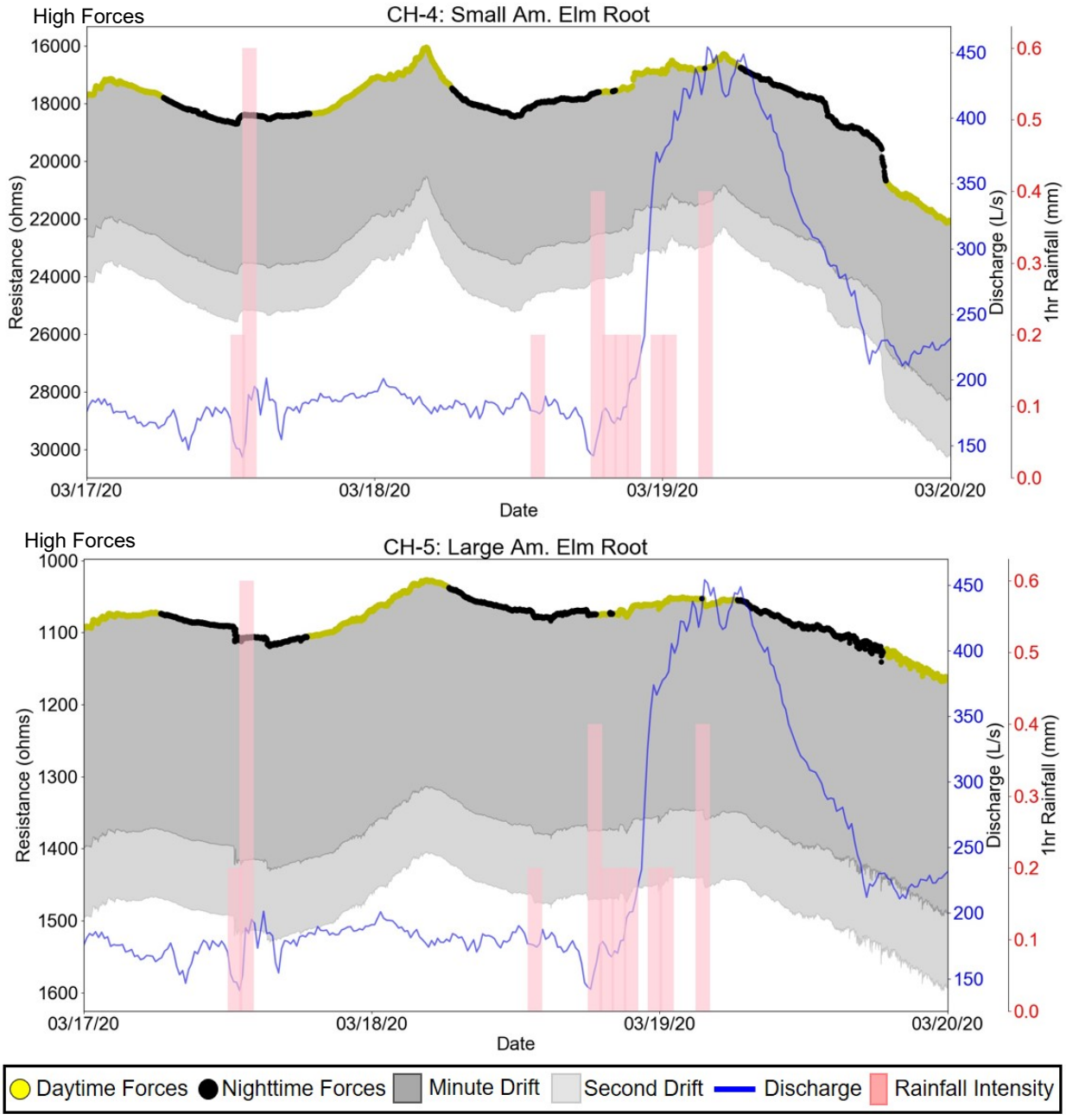

Figure 15. Changes in root forces on the bedrock for American elm roots (CH-4 and CH-5) over three days that experienced heavy rainfall followed by a large increase in discharge. Yellow line indicates forces when solar radiation is active and black when it is absent. The grey region indicates the uncertainties in the possible range of calibrated force-resistance curve values due to sensor drift under static loads over one-second (light grey) and one-minute (dark grey) log intervals.

After January, the diurnal variation in forces for the small American elm root (CH-4) was lessened and responded similarly to CH-7. Few direct increases in force related to individual rainfall events occurred, but forces increased throughout the night and remained more constant rather than experiencing the normal nighttime decrease when rainfall occurred at night. Forces remained much more constant when it rained compared to CH-7 then began to decrease a few hours later (Fig. 15). During January, CH-4 diurnal variation in forces was diminished, then returned to normal a few hours after rainfall. When rainfall occurred at least two days after the first heavy rainfall day, forces remained relatively constant and the diurnal variation was still gone, until a few hours after the last rainfall. The large American elm root (CH-5) responded much less to rainfall than the other roots. The diurnal variation in forces was lessened in response to rainfall during the fall and winter, and transitioning into February, diurnal variations were less impacted, however, forces at night tended to stay constant instead of decreasing (Fig. 15). Slight increases in forces during the day were observed when it rained and the typical nighttime decrease in forces was stopped when it rained during the night, yet no large increases in forces resulted from rainfall events (Fig. 15).

Following heavy rainfall events, discharge at the nearby Copperhead spring increased greatly depending on the amount of precipitation and hence, the amount of water draining to the spring (Fig. 14, 15). Forces exerted by all roots, similarly, responded to heavy rainfall events typically by increasing forces and/or a weakening in the daily cycle (Fig. 14, 15). Roots CH-4, -5, and -7, all exhibit an increase in forces approximately 2 -3 hours following rainfall events that coincided with a secondary increase in the discharge (Fig. 14, 15). Yet, no other significant trends emerged between root forces and discharge variations. Furthermore, the forces exerted by the large American elm root and the far Hackberry root showed the strongest correlation between each other amongst roots in the study, while the small American elm root was slightly

less correlated with both roots. The close Hackberry root did not correlate well with any of the other roots or environmental variables (Appendix 3.1).

4. Discussion

In this section, I first discuss the daily and seasonal patterns of root forces, specifically looking into the role of temperature and solar radiation on tree transpiration, the potential freezing of sap within the tree, and differences between species. Next, I discuss how rooting strategies between species and the roles of individual roots dictate wind-induced fluctuations in root forces exerted on the bedrock. The third section examines rainfall-induced variations in root forces, exploring how precipitation causes root forces exerted on the bedrock, as well as differences between individual root function and species. Finally, I investigate projected climate change in Northwest Arkansas and its implications on root-generated damage to bedrock via subcritical and critical cracking.

4.1 Daily and Seasonal Patterns of Root Forces

Throughout the study (which does not include the summer months), longer periods of solar radiation and stronger solar radiation, as well as longer periods of higher than average daily forces in the fall and spring occurred. This suggests that during warmer periods of more available sunlight for transpiration and water-uptake lead to lengthier periods of increased forces on the bedrock. Additionally, the trees leafing out and being more active in the fall and towards the end of the spring, supports that the roots are becoming more active on a daily basis and exerting more forces on the bedrock in response to diurnal variations in water uptake. Higher than average root forces begin to occur between the hours of 10:30 – 13:00, while solar radiation began between 5:30 – 7:00 throughout the study (Fig. 10). This suggests that the trees studied do not begin to exert higher forces on the bedrock until 4 – 5 hours following sunrise and associated photosynthetically active radiation. As detailed below, I propose that significant water stress due to transpiration and higher solar radiation is required for roots to begin exerting

forces on surrounding rock in response to daily water uptake and that they continue to exert forces on the bedrock for anywhere from 2 - 4 hours following sunset, as the tree is still taking up water in response to the water loss that occurred during the day.

4.1.1 Transpiration

Tree water transport research has documented that there is a lag in the rate of water absorption with the rate of transpiration during daylight hours (Meyer et al. 1973). Peak absorption rates of water from roots occur later in the day than peak transpiration rates and the rate of absorption is continuously higher than transpiration at night, although typically lower than the normal daytime rate of water absorption (Meyer et al. 1973). Water continues to move upwards in the tree during the night hours after transpiration has ceased due to the residual negative water potentials of the leaf cells from the previous day (Meyer et al. 1973). This suggests that as the tree roots absorb water from the soil or rock, lagging a few hours behind solar radiation, they exert higher than average daily forces on the bedrock from midday hours through the night. Furthermore, as the seasons' transition from fall to winter, when solar radiation and temperature, the two most influential controls on transpiration, are the lowest, we see a decreased period of root forces being exerted on the surrounding bedrock. During the spring months, solar radiation becomes stronger and occurs for longer periods of time, while temperatures become higher, and the trees begin to bloom again, which results in longer periods of higher root forces being exerted on the bedrock. These months of longer periods of forces being exerted correspond with the typical blooming times of both trees, where American elm trees begin to bloom between March and April while Hackberry trees bloom between April and May (Missouri Botanical Garden, 2020). While the American elm blooms before the Hackberry in general, visits to the field site indicated that both trees did not begin to grow leaves until approximately the same time in April.

Throughout the study, the strongest correlation occurred between temperature and all root forces except for the root instrumented close to the Hackberry tree (CH-1) (Appendix 3.1). For all roots during nearly every month, the timing of daily minimum and maximum daily peaks in force occurred anywhere from a few minutes to an hour before peaks in temperature (Fig. 10, Table 3, 4). This suggests that temperature via transpiration is the dominant environmental control on diurnal variations in forces during the fall through spring months, which constitute the period of this study. Also, rises in temperature lead to an increase in the vapor gradient through the stomate of the leaf, resulting in an increasing transpiration rate (Meyer et al. 1973). While many studies on the daily cycles of tree stem diameter variations in response to tree transpiration have found that trunks and roots expand during the night and shrink during the day, as transpiration demands exceed the water storage of the tree and refill during the night causing an expansion (Zweifel et al., 2001; Steppe et al., 2006), our results suggest an inverse trend that is heavily temperature-dependent. Similarly, studies including King et al. (2013), Turcotte et al. (2009), and Wang et al. (2012) have demonstrated in their findings that during fall, winter, and early spring months, diurnal stem and root diameter variations for both deciduous and evergreen trees experience an inverse diurnal cycle that was heavily dependent on changes in temperature.

During the winter, there is a phase shift in the daily cycles of the maximum stem and root size to the late afternoon, suggesting that transpiration is no longer the primary driver of diurnal cycles in the winter and that temperature becomes the main factor in stem and root size fluctuations (Sevanto et al., 2006; King et al., 2013). While they observed this shift in diurnal variations from November through March (Turcotte et al., 2009; King et al., 2013), the roots in this study displayed this pattern primarily from October through April (Fig. 8). Seasonal changes in root diameter growth cycles are typically divided into three periods throughout the year that consist of winter shrinkage, spring rehydration, and summer transpiration (Turcotte et al., 2009).

The winter shrinkage cycle, typically beginning around November corresponds to a decrease in root radius and is associated with the onset of cold temperatures (Turcotte et al., 2009). During this time, as air and soil temperatures decrease, the normal diurnal cycle of root expansion at night and shrinking during the day is replaced by an inverted cycle. This is associated with nighttime shrinkage and daytime swelling of plant tissues, that are primarily controlled by temperature (Zweifel and Häsler, 2000; Tardif et al., 2001). Large increases and decreases of root forces (Fig. 16) associated with large temperature changes, were also found by Turcotte et al. (2009) in stem variations, yet they did not identify them in root diameter variations as their study location had snowfall which insolated the roots from these large fluctuations. The lack of snowfall during our study suggests that in regions that experience cold temperatures with an absence of snowfall, diameter variations in roots will be dramatically affected by fluctuations of air temperatures as there is no snow cover insolating the roots from the effect of temperature. This is further supported as Turcotte et al. (2009) found that even during the summer transpiration phase, the occurrence of cold temperatures caused a shift from normal daily diameter cycles back to an inverse cycle primarily in roots rather than in the stem after the snow cover was melted.

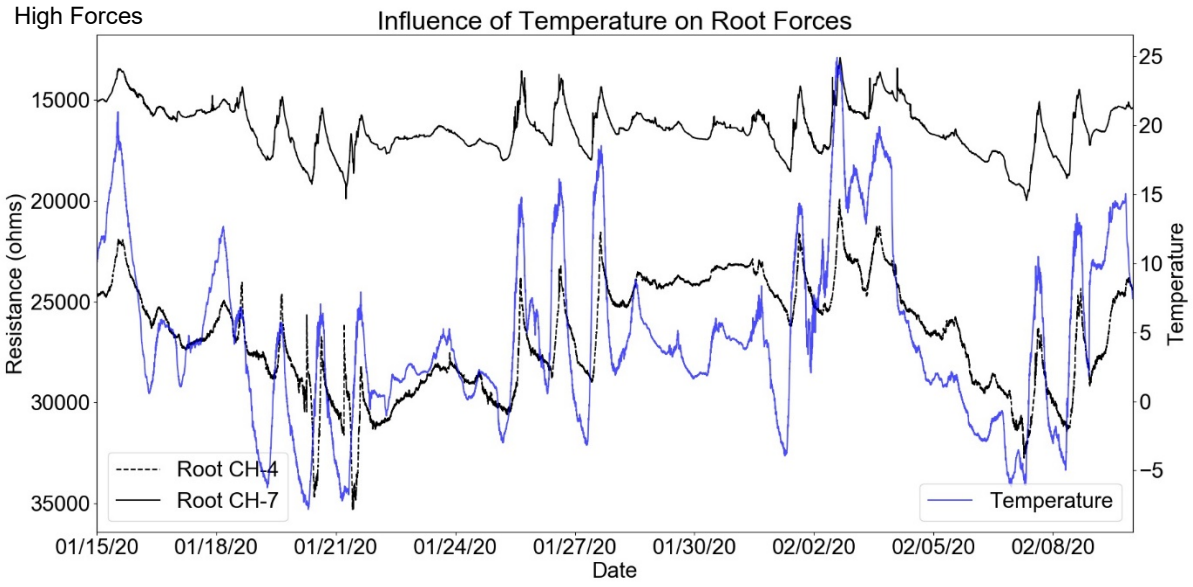

Figure 16. Root forces for both Hackberry (CH-7) and American elm (CH-4) with temperature (blue line) from January 15 – February 7, 2020, during periods of both high and low temperatures.

4.1.2 Sap-freezing

Changes in diurnal stem and root diameter examined in the winter have often been attributed to osmotic water movement caused by temperature changes around the freezing point of sap (Mayr et al., 2006). It is suggested that as the temperature reaches below approximately -5 °C, the extra-cellular water begins to freeze which initiates osmotic withdrawal of inter-cellular water that causes the stem and roots to shrink (King et al., 2013; Turcotte et al., 2009). As temperatures rise during the day, this process is reversed and water starts to flow back into the cells, inducing stem and root expansion which dictates the daily maximum peak in the stem or root diameter (King et al., 2013; Turcotte et al., 2009). At this study's location, temperatures did reach the sap freezing temperature, but not often and not during many of the months where this shifted diurnal cycle was experienced. King et al. (2013) found that at the site where temperatures rarely reached this sap-freezing temperature, the phase shift was relatively absent, suggesting that other factors may be causing this daily cycle at our site besides the freezing and thawing of sap within the tree.

4.1.3 Species Differences

Qualitatively analyzing diurnal changes in root forces throughout the study, during periods of higher temperature and solar radiation, root forces have a greater amplitude (Fig. 16). As temperatures and solar radiation decreased and remained lower as well as a reduction in plant growth during the winter, daily amplitudes in root forces become much smaller (Fig. 16). King et al. (2013) attributed this observation to increased canopy transpiration rates and water demands of the trees. The lack of correlation between the close Hackberry root (CH-1) and temperature (Appendix 3.1) and the generally smaller daily amplitudes in root forces suggests that roots located closer to the stem of this species may not be exploiting their internal water reserves as quickly. In contrast, the American elm root monitored closer to the tree experienced large daily amplitudes and was highly temperature-dependent suggesting this species may be able to access it's internal water reserves. King et al. (2013) hypothesized that differences between the amplitude of stem diameter variations of species may be related to their root systems, where trees with deeper root systems can access additional soil water resources and rely less on their internal water reserves, resulting in smaller daily amplitudes in stem diameter fluctuations. Hackberry trees are considered more drought-resistant, having relatively deep root systems (Sprackling and Read, 1979), which suggest that this tree has deeper roots available to access soil or rock moisture and may explain that lack of large diurnal variation in root forces and lack of correlation with temperature. Conversely, American elm is a bottomland species that is not drought-resistant, with below-average depth/height ratios (Sprackling and Read, 1979). American elm trees have comparatively shallow and narrow root systems (Sprackling and Read, 1979), positing that they may access their internal water reserves more quickly which could explain why both roots (CH-4 and CH-5) correlated strongly with temperature and experienced greater daily amplitudes in forces as temperatures increased. Although these species are known to exhibit different rooting strategies in soils, the extent of each species rooting depth in

this bedrock dominated environment is speculative without knowing how rooting depth may vary between soil or bedrock landscapes. Differences among species' hydraulic strategies promote varying rates and patterns of transpiration, and it is not uncommon for trees of different species within the same ecosystem to employ opposing hydraulic strategies which have been largely linked variations in the rooting depth of co-occurring species, enabling drought-resistant species to access pools of water underground that may be unavailable to other nearby species (Canadell et al., 2007; Matheny et al., 2017). These findings suggest that in less drought-tolerant species with shallow root systems, as large temperature-driven transpiration demands cause the roots to contract and expand more during the day, the larger variations in diurnal forces associated with temperature and transpiration may induce larger forces on the bedrock (Canadell et al., 2007; Matheny et al., 2017).

4.2 Wind-induced Fluctuations in Root Forces

Although there was not an extremely strong response between wind events and any of the roots in the study, there is an evident difference in response between species and roots for each tree. The roots of the American elm tree demonstrate a relatively elastic response to wind gusts with more frequent fluctuations in forces while the roots of the Hackberry tree display a stiffer response to wind gusts exhibiting larger response to individual wind events. (Table 1) The American elm tree has a smaller DBH, and its wood is less dense, having a higher modulus of elasticity (Table 1). The Hackberry tree is much taller, with a larger DBH, and denser wood (Table 1). Furthermore, the Hackberry tree with an estimated truck mass nearly five times greater than the American elm and thus likely have a greater root system, presumably more structurally stable, with the roots only occasionally being affected by wind gusts. Additionally, given that the location of the roots I monitored on the American elm tree was closer to the truck of the smaller tree than those I monitored on the American elm, I speculate that proximal roots would likely record an increased response to wind.

The large American elm root (CH-5) exhibited the largest fluctuations of forces in response to wind gusts in this study with forces fluctuating as wind gusts exceed 6 m/s, becoming larger as wind gusts increased. While the smaller, closer root (CH-4) below the tree exhibited smaller fluctuations in forces when wind gusts exceed 10 m/s during the day and when gusts exceed 6 m/s at night. The difference in responses between these roots can likely be attributed to their role and location relative to the dominant wind direction. The larger root was the only northeast-facing root of the study, hence being the only windward root for any of the trees in the study, as the dominant wind direction at this location is south/southwest throughout the whole study period. Given that large lateral roots coming directly off the trunk of the tree tend to provide much of the stability for trees, with windward facing roots providing much more stability than the other roots of the tree (Coder, 2010). My data suggests this may be the primary function of the large American elm root.

The root of the Hackberry tree monitored closer to the trunk (CH-1) showing smaller fluctuations in forces on the bedrock when wind gusts exceed 8 m/s and the root monitored nearly 4 m away from the trunk (CH-7) showing slightly larger fluctuations only during sustained wind gusts of 4 – 6 m/s, present an interesting find within my study. While it would be expected that the root instrumented at a closer location would respond more often, both roots show an overall very weak response to wind events. While wind-driven fluctuations in forces on the bedrock were very small, subcritical cracking is additive and the supplement of temperature and moisture-driven stresses on the rock (Eppes et al., 2016) as well could lead to significant damage to the surrounding bedrock over the lifetime of the tree (> 100 years). I further suggest that for species similar to American elm that exhibit a more elastic response to wind gusts, exerting constant fluctuations in root-forces on the bedrock for many hours may exert a greater degree of subcritical stresses on the rock, contributing to even greater rock damage over the lifetime of the tree.

These differences in responses between the roots of different species may be a result of each species' rooting system (McElrone et al., 2004). The higher response of the large lateral American Elm root is likely attributed to the shallow lateral root system of American Elm trees, especially in regions which high water-tables (Sprackling & Read, 1979) such as the Savoy Experimental Watershed, where the water table is near the surface. With most of the root system being shallow and spread laterally, these surface lateral roots, specifically the American elm roots in this study that were both instrumented within 1.5m of the tree base, likely experience much more movement in response to wind gusts (Coder, 2010). However, without direct measurements of the rooting system belowground, this can only be a hypothesized finding.

4.3 Rainfall-induced Variations in Root Forces

For all roots, rainfall events caused smaller amplitudes in daily forces, yet each responded slightly differently at the hourly scale. The large American elm root (CH-5) displays sharp decreases with each rainfall event followed by a relatively constant trend in forces on the bedrock, which indicates that the amplitude of the diurnal cycle of forces is being subdued. This suggests two hypotheses: 1) this large lateral root is primarily used for stability as it is growing upslope of the tree, further from the water table; or 2) while precipitation increases soil water availability, the branches, smaller roots, and leaves are directly intercepting and absorbing rain, reducing the need for the tree to need to access soil or rock water uptake at this location. The data from the smaller American elm root (CH-4) does show increases in forces exerted on the bedrock directly following rainfall, with gradual increases in forces that follow, which could be attributed to the root replenishing the water reserves in the tree as the soil moisture increases following the rainfall event (King et al., 2013). Thus, the large root function for stability rather than water-uptake is the more likely scenario to explain the difference in response between these roots (Coder, 2010).

The weakened diurnal cycle of forces in response to greater amounts of precipitation was also observed by Turcotte et al. (2011), where contraction of the root is paused, and the root diameter begins to expand in size. While these studies monitored roots growing into soils, where roots are growing into bedrock (i.e. this study), this expansion of root diameters would lead to increased pressures on the bedrock. During rainy periods, clouds can reduce radiation and VPD which decreases the transpiration of the tree and hence, the demand for water from the leaves (Turcotte et al., 2011). These long cycles that form in response to precipitation are observed in most studies on tree stem diameter changes as well as with root diameter changes (i.e. Turcotte et al., 2011). While we hypothesized that rainfall would cause the roots to swell and exert higher forces on the bedrock, our results suggest there a variation in responses for roots, where the Hackberry root instrumented closer to the trunk exhibits high forces during these long cycles, while the Hackberry root instrumented further away and the small American elm root exhibited relatively higher forces, and the large American elm root exerts longer periods of lower forces.

The differing responses experienced between species, with generally higher magnitude forces occurring with the Hackberry tree following rainfall events could again be due to the species rooting strategies. Bottomland species such as American elm which are less drought-resistant with relatively shallow root systems while Hackberry trees develop an extensive strong lateral root system as the tree becomes more mature, having developed most of its deep roots during the first ten years of growth (Sprackling & Read, 1979). Tree water supplies are replenished by root water-uptake from the upper layers of the soil/bedrock profile and the more extensive rooting system of the Hackberry tree may allow this tree to access more water from the subsurface soil-filled cavities and in the porous limestone as the soil is very shallow here and there is likely not much storage for water within this layer of epikarst (Jackson et al., 1999; Querejeta et al., 2007; Schwinning, 2010). Furthermore, with the American elm tree being

located above the Copperhead Spring cave and at a slightly higher elevation above the water table, the shallow root system may prevent some of the roots, specifically structural roots from access water within the soil following the rainfall.

Discharge of the nearby Copperhead Spring does increase in response to heavy rainfall events, yet there were no indications that the discharge influenced the root forces exerted on the bedrock (Fig. 14, 15). The increase in forces that occurred with roots CH-4, -5, and -7 that correspond to secondary increases in discharge approximately 2 -3 hours following rainfall events indicate there may be an influence on root forces associated with the lag of water transported from the head of the basin to the spring. However, it is ambiguous based on the data if the post rainfall increase in forces is a result of the timing of discharge to the spring or the lag in water-uptake from the roots in response to water being infiltrated to the subsurface. Studies have found that tree roots in karst regions take up water from caves beneath them (McElrone et al., 2004), however, I was not able to monitor roots that were accessing portions of the cave or spring. The small sample size of roots (n=4) and their surficial location and distance from the spring likely provides a bias in the attempt to link root forces to variations in spring discharge.

4.3.1 Climate Change and Subcritical Cracking

All of the roots (except the large American elm root hypothesized to function primarily as the structural support of the tree), exhibit much higher forces being exerted on the bedrock overall in response to intense rainfall and when multiple rainfall events occur for consecutive days. Precipitation indices for this location (Zhang and Yang, 2004) including maximum 5-day precipitation amount (Rx5day), simple daily intensity index (SDII), and extremely wet days (R99p) all show strong increasing trends since 1980 (Fig. 17, 18, 19), indicating that more intense precipitation has been occurring over the past 40 years (Appendix 2). Trends of increased intense precipitation and higher forces exerted by roots on bedrock in response to

intense rainfall events imply that as the climate continues to change towards conditions of more intense rainfall events, we should expect an increased frequency of rainfall-driven forces on the bedrock. Subcritical forces work over long periods of time, relying on frequent small forces on the bedrock, as more rainfall-induced- high force events increase with intense rainfall the rate of rock damage may be increased in this region. However, although more intense rainfalls are expected to occur, there is no evidence that overall precipitation amounts throughout the year will increase. This has considerable implications towards the mechanical weathering processes on the rock as warmer and wetter conditions can increase the rate of subcritical stresses on the rock (Eppes and Keanini, 2017).

4.4 Sensor Uncertainty and Drift

Many complexities arise from the use of novel approaches to answer unknown geologic questions, such as using piezoelectric force sensors to measure forces exerted by roots onto bedrock. I recognize that using low-cost sensors are not ideal for accurate measurements and not designed to provide long-term precision, however, they offer many benefits such as not disturbing the tree or rock being monitored and allow for measurements to be collected from multiple roots. While the measurements are not precise and the magnitude of forces cannot be accurately determined, the sensors provide a good temporal signal of the forces experienced at the root-rock interface. Accounting for the temperature sensitivity also demonstrates that the signal is not due to sensor response to temperature but rather tree response to variables such as VPD, solar radiation, water-uptake, and wind.

Although I could not account for all the types of static forces and the time periods over which they occur during the calibration process to accurately determine the drift time scale of the sensors, this study reveals many insights into the timing over which tree-driven forces occur in a temperate, humid environment. This will enable future work to better account for the timing of loads experienced in the field so that accurate calibration of sensors can be conducted to

determine more accurate forces on the rock exerted by tree roots. The multitude of forces including those generated by wind gusts, rainfall-induced water uptake, and daily cycles of forces from tree transpiration and nighttime water uptake provide may different timescales at which static forces can occur on the rock. This encourages interdisciplinary work between researchers such as foresters, biologists, and eco-hydrologists who study tree responses to wind and water-uptake by roots so that known time periods of these forces can be accurately determined prior to deployment of sensors in the field and minimize the uncertainty of the drift values measured.

5. Future Research

This section identifies the limitations of our study and offers suggestions on how to better identify the processes that contribute to tree-driven stresses that could damage bedrock.

1) This study primarily relies on assuming the timing of tree-water uptake in response to radiation –signaling diurnal water-uptake and rain events, yet the timing and influence of water availability for the trees at Savoy Experimental Watershed cannot be precisely determined. Future work should utilize multiple sap-flow meters and dendrometers located on the roots and on the tree stem to more precisely identify the diurnal fluid fluxes in the trees as well as the contribution of rainfall fluid to the roots which lead to swelling induced forces on the bedrock.

2) Acoustic emission (AE) sensors have been previously used by Eppes et al. (2016) on boulders to identify cracking events within the rock due to environmental stresses. Marshall and Eppes (2019) used AE sensors installed on the bedrock in conjunction with force sensors installed at the root-rock interface to identify cracking events that result both from tree processes, environmental stresses, and the combination of both (Marshall et al., 2019). By incorporating this method, it would be easier to identify cracking events in the rock caused by

tree-driven stresses, differentiate environmental stress-induced cracking from tree-induced cracking, and finally, determine how the combination of both tree-driven stresses and environmental stresses (i.e. temperature and moisture) contribute to cracking bedrock.

3) Ground-penetrating radar (GPR) has been shown to be an effective method to image the extent of tree root systems in soil and shallow bedrock, as the moisture and density of roots show a strong contrast with the surrounding soil and rock (e.g. Roering et al., 2010). Roering et al. (2010) utilized this method to determine large roots at depths as great as 3 m in thin soils (~ 40 cm), proving that tree roots can occupy bedrock beneath the trees for many meters. Future work conducting GPR imaging at Savoy Experimental Watershed (e.g. Roering et al., 2010) would allow for the determination of the extent of the rooting systems for each of these trees within the bedrock, proving a proxy for the amount of bedrock that has the ability to be disturbed by tree-driven stresses that can damage or break-up bedrock.

4) Accelerometers located at the base of the tree stem can be used to detect tree sway movement caused by wind gusts (James et al., 2006; Selker et al., 2011; van Emmerik et al., 2017; Gougherty et al., 2018). Future work using accelerometers would offer the ability to more precisely observe if the tree is experiencing movement at the base during wind events. Tree sway measurements at the base of the tree would allow for more accurate determination if the tree is experiencing movement at the near-surface during periods of higher forces measured by the forces sensors on the roots. This would allow for the determination of tree sway in response to wind gusts is the driver of higher frequency forces that the roots are exerting during wind gusts, as well as determine how the trees are individually responding to wind gusts. Tree acceleration at the base of the trunk needs to be evaluated with the tree trunk and root forces to discern how much tree trunk movement from wind gusts translates into below-ground root movement, exerting forces on the surrounding bedrock.

5) After tree forces on to the bedrock and tree sway frequencies are quantified, trail-cameras can be set up near each tree, with a camera facing the base and another facing the stem of the tree. Trail cameras offer the ability for long-term continuous monitoring of each tree. Trail cameras could prove essential to capture tree-sway movement on the video to compare with sway frequencies recorded by the accelerometers and the magnitude of root forces with the FlexiForce sensors to establish relationships between varying tree responses to wind and their resulting below-ground forces. Capturing video and extracting the spectral signature of frequency or magnitude of tree-sway will allow for studies such as this one to be upscaled to large forest swaths in the future without having to install sensors at each tree individually.

6. Conclusions

Tree roots for both American elm and Hackberry species in this study exerted higher daily forces on the bedrock for longer periods during the fall and spring compared to the winter. American elm roots and the Hackberry root instrumented 4 m away from the tree correlated strongly with temperature and maximum and minimum daily peaks coincide with the maximum and minimum daily peaks in temperature. Daily cycles of root forces exerted on the bedrock were primarily controlled by vapor pressure gradients caused by daily cycles of temperature during fall, winter, and early spring months. Hackberry tree roots with deeper root systems and being more drought-resistant correspond less to temperature and vapor pressure demands.

Hackberry roots exhibited a stiff response to the wind as the tree is larger, has denser wood, and is known to have a more extensive root system to support the tree. American elm roots displayed an elastic response to wind gusts, fluctuating more often as the tree is smaller, less dense, and has a shallower root system as well as the roots being in closer proximity to the trunk. The stiff response of the Hackberry tree with discrete fluctuations in forces may not lead

to as much bedrock damage as compared to the elastic response of the American elm roots which can exert fluctuations in forces for many hours.

Spring discharge and root forces both displayed an increase in response to heavy rainfall events, yet these processes do not appear to be linked to each other and are both a result of precipitation. The amplitude of the diurnal cycle of forces exerted on the bedrock is diminished for all roots in response to heavy rainfall or rainfall occurring for multiple days. This can be attributed to a combination of factors including the swelling of roots due to water uptake, but primarily to cloud formation that reduces solar radiation and VPD which decreases the transpiration of trees. Intense rainfall events are forecasted to occur in this area in the future, suggesting that trees such as Hackberry will exert more of these higher root force events in response to intense precipitation.

The findings of this study suggest that both American elm and Hackberry roots have the ability to exert subcritical forces on the surrounding bedrock on a variety of timescales in response to environmental conditions. The contribution of small fluctuations in forces on a sub-hourly scale to wind gusts, increases in forces in response to rainfall events as roots swell, as well as daily increases in forces from midday through night hours, have the ability to significant subcritical stresses on the bedrock. The additive combination from daily temperature stresses, rock moisture stresses, as well as warmer and wetter conditions resulting from climate change, suggests that tree roots growing into bedrock may significantly increase the rate of subcritical cracking, which drives the mechanical weathering of rocks and proves to be a great contribution towards soil production over the lifetime of a tree in bedrock-dominated environments.

7. References

Anderson, S.P., 2019, Breaking it Down: Mechanical Processes in the Weathering Engine: Elements, v. 15, p. 247–252, doi:10.2138/gselements.15.4.247.

Atkinson, B.K., 1984, Subcritical crack growth in geological materials: Journal of Geophysical Research: Solid Earth, v. 89, p. 4077–4114, doi:10.1029/JB089iB06p04077@10.1002/(ISSN)2169-9356.CHEMDEF1.

Brahana, J.V., Hays, P.D., Kresse, T.M., Sauer, T.J., and Stanton, G.P., 1999, The Savoy Experimental Watershed–Early Lessons for Hydrogeologic Modeling From a Well-Characterized Karst Research Site: Karst modeling, Karst Waters Institute Special Publication, v. 5, p. 247–254.

Brantley, S.L. et al., 2017, Reviews and syntheses: on the roles trees play in building and plumbing the critical zone: Biogeosciences, v. 14, p. 5115–5142, doi:10.5194/bg-14-5115-2017.

Canadell, J.G., Pataki, D.E., and Pitelka, L. (Eds.), 2007, Terrestrial ecosystems in a changing world: Berlin ; New York, Springer, Global change--the IGBP series, 336 p.

Celtis occidentalis - Plant Finder, https://www.missouribotanicalgarden.org/PlantFinder/PlantFinderDetails.aspx?kemperco de=a858 (accessed June 2020).

Chave, J., Coomes, D., Jansen, S., Lewis, S.L., Swenson, N.G., and Zanne, A.E., 2009, Towards a worldwide wood economics spectrum: Ecology Letters, v. 12, p. 351–366, doi:10.1111/j.1461-0248.2009.01285.x.

Coder, K.D. Root Strength & Tree Anchorage: University of Georgia Warnell School of Forestry & Natural Resources monograph publication WSFNR10-19*, p. 88.

Dietrich, W.E., and Perron, J.T., 2006, The search for a topographic signature of life: Nature, v. 439, p. 411–418, doi:10.1038/nature04452.

van Emmerik, T., Steele-Dunne, S., Hut, R., Gentine, P., Guerin, M., Oliveira, R., Wagner, J., Selker, J., and van de Giesen, N., 2017, Measuring Tree Properties and Responses Using Low-Cost Accelerometers: Sensors, v. 17, p. 1098, doi:10.3390/s17051098.

Eppes, M.-C., and Keanini, R., 2017, Mechanical weathering and rock erosion by climate-dependent subcritical cracking: WEATHERING BY SUBCRITICAL CRACKING: Reviews of Geophysics, v. 55, p. 470–508, doi:10.1002/2017RG000557.

Eppes, M.C., Magi, B., Hallet, B., Delmelle, E., Mackenzie-Helnwein, P., Warren, K., and Swami, S., 2016, Deciphering the role of solar-induced thermal stresses in rock weathering: Geological Society of America Bulletin, v. 128, p. 1315–1338, doi:10.1130/B31422.1.

Estrada-Medina, H., Graham, R.C., Allen, M.F., Jiménez-Osornio, J.J., and Robles-Casolco, S., 2013, The importance of limestone bedrock and dissolution karst features on tree root distribution in northern Yucatán, México: Plant and Soil, v. 362, p. 37–50, doi:10.1007/s11104-012-1175-x.

Gabet, E.J., and Mudd, S.M., 2010, Bedrock erosion by root fracture and tree throw: A coupled biogeomorphic model to explore the humped soil production function and the persistence of hillslope soils: Journal of Geophysical Research, v. 115, doi:10.1029/2009JF001526.

Goodfellow, B.W., Hilley, G.E., Webb, S.M., Sklar, L.S., Moon, S., and Olson, C.A., 2016, The chemical, mechanical, and hydrological evolution of weathering granitoid: Journal of Geophysical Research: Earth Surface, v. 121, p. 1410–1435, doi:10.1002/2016JF003822.

Gougherty, A.V., Keller, S.R., Kruger, A., Stylinski, C.D., Elmore, A.J., and Fitzpatrick, M.C., 2018, Estimating tree phenology from high frequency tree movement data: Agricultural and Forest Meteorology, v. 263, p. 217–224, doi:10.1016/j.agrformet.2018.08.020.

Hammer, O., Harper, D.A.T., and Ryan, P.D., 2010, PAST: Paleontological Statistics Software Package for Education and Data Analysis: , p. 9.

Harrison, R., Footen, P., and Strahm, B., 2011, Deep Soil Horizons: Contribution and Importance to Soil Carbon Pools and in Assessing Whole-Ecosystem Response to Management and Global Change: Forest Science, v. 57, p. 67–76.

Hasenmueller, E.A., Gu, X., Weitzman, J.N., Adams, T.S., Stinchcomb, G.E., Eissenstat, D.M., Drohan, P.J., Brantley, S.L., and Kaye, J.P., 2017, Weathering of rock to regolith: The activity of deep roots in bedrock fractures: Geoderma, v. 300, p. 11–31, doi:10.1016/j.geoderma.2017.03.020.

Jackson, P.C., Meinzer, F.C., Bustamante, M., Goldstein, G., Franco, A., Rundel, P.W., Caldas, L., Igler, E., and Causin, F., 1999, Partitioning of soil water among tree species in a Brazilian Cerrado ecosystem: Tree Physiology, v. 19, p. 717–724, doi:10.1093/treephys/19.11.717.

James, K.R., Haritos, N., and Ades, P.K., 2006, Mechanical stability of trees under dynamic loads: American Journal of Botany, v. 93, p. 1522–1530, doi:10.3732/ajb.93.10.1522.

King, G., Fonti, P., Nievergelt, D., Büntgen, U., and Frank, D., 2013, Climatic drivers of hourly to yearly tree radius variations along a 6°C natural warming gradient: Agricultural and Forest Meteorology, v. 168, p. 36–46, doi:10.1016/j.agrformet.2012.08.002.

Marshall, J.A., 2018, From ice to trees, surprising insights into past and present processes that sculpt our earth: AGU Fall Meeting Abstracts, v. 44, http://adsabs.harvard.edu/abs/2018AGUFMEP44A..01M (accessed March 2019).

Marshall, J.A., Eppes, M.C., and Mhatre, K., 2019, Listening for how trees, wind, water, and temperaturepropagate and amplify near-surface fracturing: GSA Annual Meeting in Phoenix, USA-2019,.

Matheny, A.M., Fiorella, R.P., Bohrer, G., Poulsen, C.J., Morin, T.H., Wunderlich, A., Vogel, C.S., and Curtis, P.S., 2017, Contrasting strategies of hydraulic control in two codominant temperate tree species: Ecohydrology, v. 10, p. e1815, doi:10.1002/eco.1815.

Matthes-Sears, U., and Larson, D.W., 1995, Rooting Characteristics of Trees in Rock: A Study of Thuja occidentalis on Cliff Faces: International Journal of Plant Sciences, v. 156, p. 679–686, doi:10.1086/297290.

Mayr, S., Wieser, G., and Bauer, H., 2006, Xylem temperatures during winter in conifers at the alpine timberline: Agricultural and Forest Meteorology, v. 137, p. 81–88, doi:10.1016/j.agrformet.2006.02.013.

McElrone, A.J., Pockman, W.T., Martinez-Vilalta, J., and Jackson, R.B., 2004, Variation in xylem structure and function in stems and roots of trees to 20 m depth: New Phytologist, v. 163, p. 507–517, doi:10.1111/j.1469-8137.2004.01127.x.

Meyer, B.S., Anderson, D.B., Bohning, R.H., and Fratianne, D.G., 1973, Introduction to plant physiology: New York, Van Nostrand Co, 565 p.

Misra, R.K., Dexter, A.R., and Alston, A.M., 1986, Maximum axial and radial growth pressures of plant roots: Plant and Soil, v. 95, p. 315–326, doi:10.1007/BF02374612.

Moore, J.R., and Maguire, D.A., 2004, Natural sway frequencies and damping ratios of trees: concepts, review and synthesis of previous studies: Trees - Structure and Function, v. 18, p. 195–203, doi:10.1007/s00468-003-0295-6.

Ni, J., Luo, D.H., Xia, J., Zhang, Z.H., and Hu, G., 2015, Vegetation in karst terrain of southwestern China allocates more biomass to roots: Solid Earth, v. 6, p. 799–810, doi:10.5194/se-6-799-2015.

Pawlik, Ł., Phillips, J.D., and Šamonil, P., 2016, Roots, rock, and regolith: Biomechanical and biochemical weathering by trees and its impact on hillslopes—A critical literature review: Earth-Science Reviews, v. 159, p. 142–159, doi:10.1016/j.earscirev.2016.06.002.

Pennington, D.W., 2010, Karst Drainage-Basin Analysis Using Hydrograph Decomposition Techniques at the Savoy Experimental Watershed, Savoy, Arkansas [Master's Thesis]: University of Arkansas.

Phillips, J.D., 2016, Biogeomorphology and contingent ecosystem engineering in karst landscapes: Progress in Physical Geography, v. 40, p. 503–526, doi:10.1177/0309133315624641.

PRISM Climate Group, Oregon State University, http://prism.oregonstate.edu, created 4 Feb 2004.

Querejeta, J.I., Estrada-Medina, H., Allen, M.F., and Jiménez-Osornio, J.J., 2007, Water source partitioning among trees growing on shallow karst soils in a seasonally dry tropical climate: Oecologia, v. 152, p. 26–36, doi:10.1007/s00442-006-0629-3.

Rempel, A.W., Marshall, J.A., and Roering, J.J., 2016, Modeling relative frost weathering rates at geomorphic scales: Earth and Planetary Science Letters, v. 453, p. 87–95, doi:10.1016/j.epsl.2016.08.019.

Riebe, C.S., Hahm, W.J., and Brantley, S.L., 2017, Controls on deep critical zone architecture: a historical review and four testable hypotheses: Four Testable Hypotheses about the Deep Critical Zone: Earth Surface Processes and Landforms, v. 42, p. 128–156, doi:10.1002/esp.4052.

Rizzo, D.M., and Harrington, T.C., 1988, Root movement and root damage of red spruce and balsam fir on subalpine sites in the White Mountains, New Hampshire: Canadian Journal of Forest Research, v. 18, p. 991–1001, doi:10.1139/x88-152.

Roering, J.J., Marshall, J., Booth, A.M., Mort, M., and Jin, Q., 2010, Evidence for biotic controls on topography and soil production: Earth and Planetary Science Letters, v. 298, p. 183–190, doi:10.1016/j.epsl.2010.07.040.

Schwinning, S., 2013, Do we need new rhizosphere models for rock-dominated landscapes? Plant and Soil, v. 362, p. 25–31, doi:10.1007/s11104-012-1482-2.

Schwinning, S., 2010, The ecohydrology of roots in rocks: Ecohydrology, p. n/a-n/a, doi:10.1002/eco.134.

Schwinning, S., 2008, The water relations of two evergreen tree species in a karst savanna: Oecologia, v. 158, p. 373–383, doi:10.1007/s00442-008-1147-2.

Selker, J.S., Lane, J.W., Rupp, D.E., Hut, R., Abou Najm, M.R., Stewart, R.D., Van De Giesen, N., and Selker, F., 2011, The answer is blowing in the wind: using wind induced resonance of trees to measure time varying canopy mass, including interception: AGU Fall Meeting Abstracts, v. 11, p. H11G-1155.

Sevanto, S., Suni, T., Pumpanen, J., Grönholm, T., Kolari, P., Nikinmaa, E., Hari, P., and Vesala, T., 2006, Wintertime photosynthesis and water uptake in a boreal forest: Tree Physiology, v. 26, p. 749–757, doi:10.1093/treephys/26.6.749.

Steppe, K., De Pauw, D.J.W., Lemeur, R., and Vanrolleghem, P.A., 2006, A mathematical model linking tree sap flow dynamics to daily stem diameter fluctuations and radial stem growth: Tree Physiology, v. 26, p. 257–273, doi:10.1093/treephys/26.3.257.

Tardif, J., Flannigan, M., and Bergeron, Y., 2001, An Analysis of the Daily Radial Activity of 7 Boreal Tree Species, Northwestern Quebec: , p. 20.

Turcotte, A., Morin, H., Krause, C., Deslauriers, A., and Thibeault-Martel, M., 2009, The timing of spring rehydration and its relation with the onset of wood formation in black spruce: Agricultural and Forest Meteorology, v. 149, p. 1403–1409, doi:10.1016/j.agrformet.2009.03.010.

Turcotte, A., Rossi, S., Deslauriers, A., Krause, C., and Morin, H., 2011, Dynamics of Depletion and Replenishment of Water Storage in Stem and Roots of Black Spruce Measured by Dendrometers: Frontiers in Plant Science, v. 2, doi:10.3389/fpls.2011.00021.

Zhang, X., and Yang, F., 2004, RClimDex (1.0) User Manual: Climate Research Brach Environment Canada, p. 23.

Zweifel, R., and Häsler, R., 2000, Frost-induced reversible shrinkage of bark of mature subalpine conifers: Agricultural and Forest Meteorology, v. 102, p. 213–222, doi:10.1016/S0168-1923(00)00135-0.

Zweifel, R., Item, H., and Häsler, R., 2001, Link between diurnal stem radius changes and tree water relations: Tree Physiology, v. 21, p. 869–877, doi:10.1093/treephys/21.12-13.869.

Zwieniecki, M.A., and Newton, M., 1994, Root distribution of 12-year-old forests at rocky sites in southwestern Oregon: effects of rock physical properties: Canadian Journal of Forest Research, v. 24, p. 1791–1796, doi:10.1139/x94-231.

8. Appendices

Appendix 1.1 Weather Station Sensor Error and Limitations

	Sensor Error	
Measurement	Accuracy	Resolution
Temperature	± 0.21°C	0.02°C
Relative Humidity	± 2.5%	0.10%
Wind Speeds	± 1.1 m/s	0.5 m/s
Wind Direction	± 5 degrees	1.4 degrees
Solar Radiation	± 10 W/m²	1.25 W/m²
Rainfall		0.2 mm

Appendix 1.2 Force Sensor Error and Limitations

FlexiForce Sensor Performance	
Error	< ± 3%
Repeatability	< ± 2.5%
Hysteresis	< 4.5%
Drift	< 5%
Response Time	< 5 µsec
Temp. Sensitivity	0.36% / °C

Appendix 2.1 Rainfall Indices Calculated in RClimDex

"ClimDex is a Microsoft Excel based program that provides an easy-to-use software package for the calculation of indices of climate extremes for monitoring and detecting climate change. It was developed by Byron Gleason at the National Climate Data Centre (NCDC) of NOAA, and has been used in CCl/CLIVAR workshops on climate indices from in 2001." (Zhang and Yang, 2004)

Appendix 2.2 List of Climate Indices

ID	Indicator name	Definitions	UNITS
Rx5day	Max 5-day precipitation amount	Monthly maximum consecutive 5-day precipitation	Mm
SDII	Simple daily intensity index	Annual total precipitation divided by the number of wet days (defined as PRCP>=1.0mm) in the year	Mm/day
R99p	Extremely wet days	Annual total PRCP when RR>99th percentile	mm

Appendix 2.3 Indices Definitions

1. Rx5day

Let RR_{kj} be the precipitation amount for the 5-day interval ending k, period j. Then maximum 5-day values for period j are:

$$Rx5day_j = \max(RR_{kj})$$

2. SDII

Let RR_{wj} be the daily precipitation amount on wet days, $w(RR \geq 1mm)$ in period j. If W represents number of wet days in j, then:

$$SDII_j = \frac{\sum_{w=1}^{W} RR_{wj}}{W}$$

3. R99p

Let RR_{wj} be the daily precipitation amount on a wet day $w(RR \geq 1.0mm)$ in period j and let $RR_{wn}99$ be the 99th percentile of precipitation on wet days in the 1961-1990 period. If W represents number of wet days in the period, then:

$$R99p_j = \sum_{w=1}^{W} RR_{wj} \text{ where } RR_{wj} > RR_{wn}99$$

Appendix 2.4 Rainfall Indices Plots

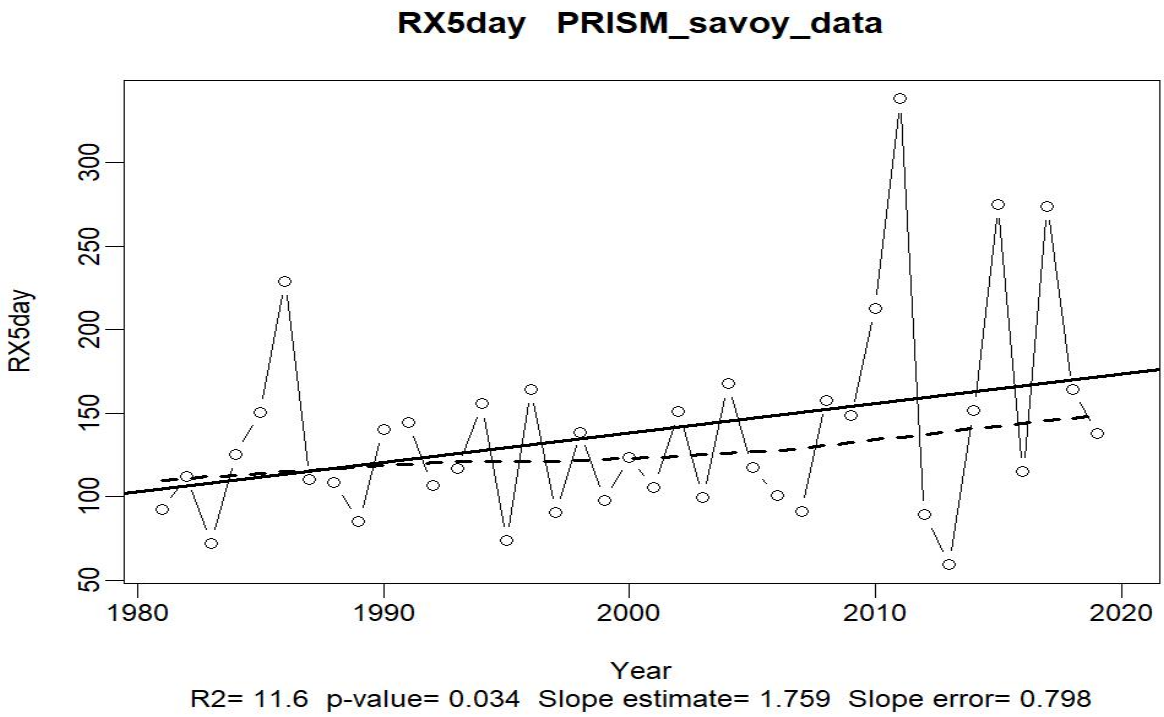

Figure 17. Maximum five-day precipitation amount (RX5day) for each year at Savoy, Arkansas from 1981 – 2019. The y-axis is the total precipitation that occurred during the five wettest days of each month for the corresponding year (mm).

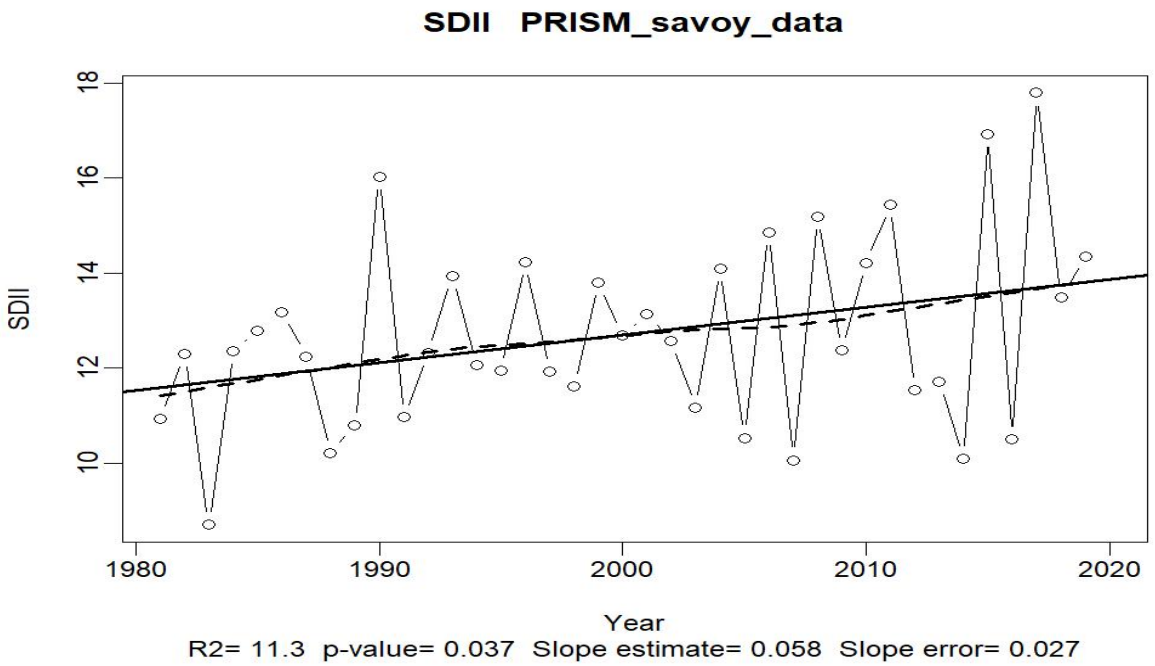

Figure 18. Simple daily intensity index (SD11) calculated for each year at Savoy, Arkansas from 1981 – 2019. The y-axis is the annual precipitation divided by the number of days when precipitation was > 1 mm for each year (mm/day).

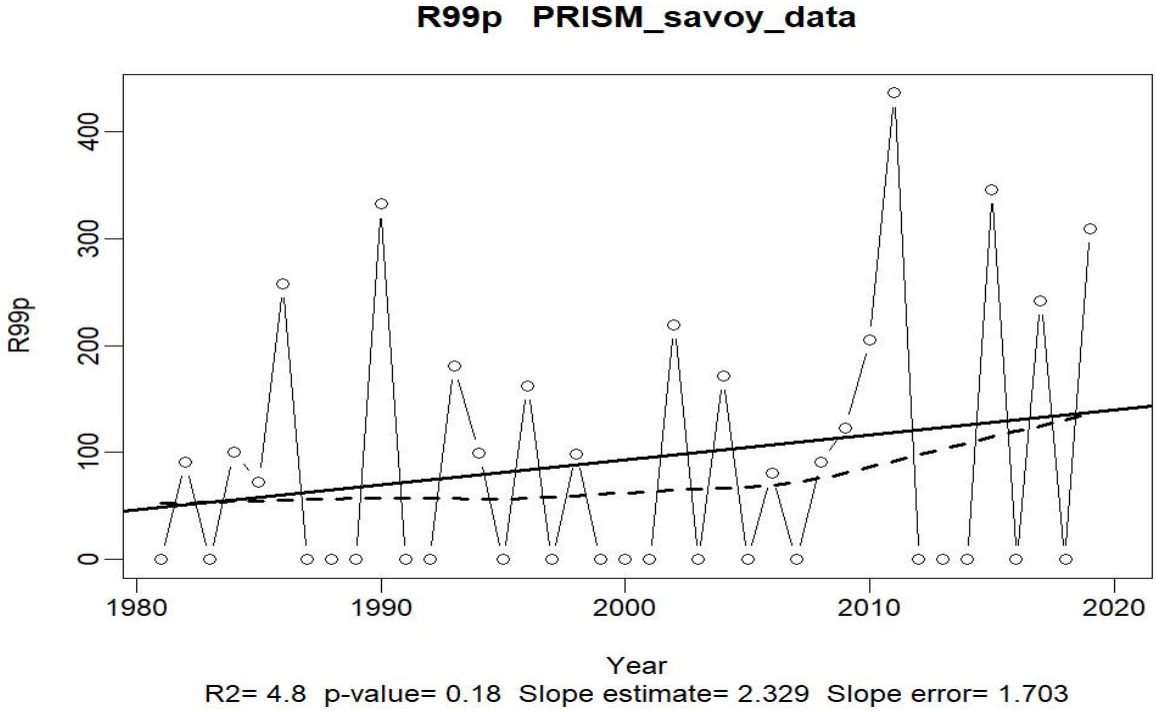

Figure 19. Extremely wet days (R99p) that occurred during each year at Savoy, Arkansas from 1981 – 2019. The y-axis is the amount of precipitation (mm) that occurred during the extremely wet days during each year.

Appendix 3.1 Monthly Correlation Tables Between Variables

September Pearson's r correlations and p-values.

	C-1	C-4	C-5	C-7	GustSpeed	RH_%	SolarRad	Temp	WaterCont	WindSpeed
C-1		0	2.8566E-19	5.585E-08	0.83552	0.00010716	6.5332E-07	8.0882E-07	7.7871E-52	3.1363E-05
C-4	0.7217		0.18945	1.1783E-48	0.00104	0.00090395	0.0012125	0.2363	2.4046E-32	5.6712E-09
C-5	0.13823	0.020308		0	0.84722	0.76941	2.2623E-09	0.0018648	3.304E-35	0.56945
C-7	-0.083919	-0.224	0.67112		2.5823E-08	1.19E-13	9.5868E-09	1.887E-26	2.0976E-12	9.4142E-06
GustSpeed	-0.0032136	0.050725	0.0029819	-0.086013		1.9845E-311	0	3.8743E-317	8.9005E-41	0
RH_%	-0.059902	0.051333	-0.0045372	0.11443	-0.53747		0	0	1.2219E-45	1.64E-222
SolarRad	0.076882	-0.050052	-0.092322	-0.088633	0.60258	-0.7373		0	3.7601E-34	2.7528E-317
Temp	0.076242	-0.018328	-0.048122	-0.16361	0.54161	-0.94287	0.80476		1.8058E-41	2.4269E-206
WaterCont	0.23127	0.18173	0.18988	0.10845	0.20476	-0.21685	0.18692	0.20653		2.9781E-49
WindSpeed	0.064371	0.089991	-0.0088044	-0.068488	0.93787	-0.46438	0.54171	0.44894	0.22538	

October Pearson's r correlations and p-values.

	C-1	C-4	C-5	C-7	GustSpeed	RH_%	SolarRad	Temp	WaterCont	WindSpeed
C-1		1.3125E-76	1.2301E-129	1.2969E-249	1.1581E-31	0.040437	0.025926	2.9404E-138	0.71103	2.7813E-17
C-4	0.27206		0	0	6.0835E-36	4.745E-13	2.0885E-05	0	0.00067673	1.3822E-20
C-5	0.35103	0.56967		0	2.2218E-06	1.2182E-42	1.0196E-05	0	0.0036218	7.5669E-09
C-7	0.47456	0.70357	0.81248		4.7758E-13	1.9269E-47	5.2201E-13	0	3.5861E-08	2.7195E-17
GustSpeed	-0.17393	-0.18573	-0.070749	-0.10794		6.5406E-299	0	4.1854E-151	0.76398	0
RH_%	0.030669	0.10795	0.20275	0.21407	-0.51343		0	7.1424E-288	0.032951	1.0869E-322
SolarRad	0.033333	-0.063634	-0.065988	-0.10776	0.57409	-0.68375		7.3621E-256	0.011022	0
Temp	-0.3619	-0.60719	-0.79317	-0.85484	0.37736	-0.50516	0.47978		0.00010301	2.1714E-148
WaterCont	-0.0055458	-0.050846	-0.043531	-0.082344	-0.0044947	-0.031917	0.038039	0.058084		0.83212
WindSpeed	-0.12607	-0.13857	-0.08633	-0.12611	0.92779	-0.53052	0.59699	0.37417	0.0031732	

November Pearson's r correlations and p-values.

	C-1	C-4	C-5	C-7	GustSpeed	RH_%	SolarRad	Temp	WaterCont	WindSpeed
C-1		1.1008E-12	0.057486	3.8541E-150	0.10575	0.10878	0.059911	1.3088E-78	0.14849	0.45973
C-4	0.15758		2.7245E-185	0	7.7317E-06	0.00067036	0.01293	5.4152E-309	3.6414E-05	0.037656
C-5	0.042304	0.58469		8.5077E-261	6.3585E-07	0.0058926	3.1897E-09	1.7594E-242	1.9987E-14	3.0495E-10
C-7	0.53561	0.7738	0.66791		0.00021235	4.4347E-24	2.0274E-05	0	2.2884E-06	0.011955
GustSpeed	0.036028	-0.0994	0.11061	-0.082382		1.3033E-65	1.6523E-121	1.6515E-12	0.0028077	0
RH_%	0.035719	0.075675	0.061295	0.22267	-0.36772		2.7169E-242	1.5103E-76	0.57805	1.1965E-57
SolarRad	-0.0419	0.055339	0.13136	-0.094741	0.48859	-0.64976		3.8328E-70	0.014885	8.1168E-104
Temp	-0.40058	-0.70982	-0.64995	-0.8998	0.15635	-0.39561	0.37961		0.0019827	3.1647E-06
WaterCont	0.032184	-0.091803	-0.16923	-0.10501	0.0665	-0.012392	-0.054216	0.068826		0.0073462
WindSpeed	0.01647	-0.046286	0.13959	-0.055957	0.96323	-0.34553	0.45537	0.10354	0.059674	

December Pearson's r correlations and p-values.

	C-1	C-4	C-5	C-7	GustSpeed_m	RH_%	SolarRad_wm	Temp_degC	WaterCont_m	WindSpeed_n
C-1		3.5219E-71	0	0	3.3544E-226	9.2048E-152	4.9364E-18	0	8.2985E-06	8.2939E-172
C-4	0.084287		0	0	0	0	1.0793E-123	0	0	0
C-5	0.31525	0.6877		0	3.7262E-52	4.1598E-166	0.75977	0	0	8.5837E-37
C-7	0.29711	0.77848	0.78688		0	0	0	0	0	0
GustSpeed_m	-0.15933	-0.3232	-0.075785	-0.37585		0	0	0	1.5775E-281	0
RH_%	0.13049	0.23838	0.13654	0.33326	-0.41064		0	0	6.814E-116	0
SolarRad_wm	-0.043203	-0.11772	0.0015271	-0.23219	0.38926	-0.49185		0	0.19315	0
Temp_degC	-0.36463	-0.73672	-0.80935	-0.83277	0.38418	-0.41752	0.38254		0	0
WaterCont_m	-0.022258	-0.22272	-0.46436	-0.50014	0.17764	-0.11391	0.0064989	0.38162		2.578E-212
WindSpeed_n	-0.13887	-0.3143	-0.063217	-0.34661	0.95827	-0.41086	0.39647	0.35154	0.15438	

January Pearson's r correlations and p-values.

	C-1	C-4	C-5	C-7	GustSpeed	RH_%	SolarRad	Temp	WaterCont	WindSpeed
C-1		0	0	0	3.6768E-209	9.1779E-59	3.443E-23	0	0.40339	2.9288E-182
C-4	0.33182		0	0	0	2.4532E-89	4.4112E-07	0	0	2.8329E-300
C-5	0.28551	0.75166		0	0	0	1.1413E-15	0	0	0
C-7	0.37816	0.6769	0.82879		0	0	0	0	3.0277E-288	0
GustSpeed	-0.14533	-0.18653	-0.30594	-0.3835		0	0	0	8.3771E-224	0
RH_%	-0.076403	-0.094657	0.20081	0.24779	-0.36423		0	0	0	0
SolarRad	0.04693	0.023904	-0.037908	-0.1995	0.28597	-0.49514		0	5.8133E-172	0
Temp	-0.30372	-0.64632	-0.84012	-0.84238	0.47219	-0.327	0.34035		0	0
WaterCont	-0.0039556	-0.24888	-0.22389	-0.1705	0.15032	-0.19226	0.13175	0.18396		5.0046E-279
WindSpeed	-0.13566	-0.174	-0.28773	-0.36203	0.9557	-0.36334	0.28117	0.43967	0.16776	

February Pearson's r correlations and p-values.

	C-1	C-4	C-5	C-7	GustSpeed	RH_%	SolarRad	Temp	WaterCont	WindSpeed
C-1		2.594E-60	0	0	0	3.1458E-15	5.2152E-12	0	0	6.9341E-223
C-4	0.080142		0	0	0	0	8.5751E-284	0	3.5866E-36	0
C-5	0.28939	0.50687		0	0	0	2.2787E-27	0	0	0
C-7	0.43663	0.61212	0.82993		0	0	0	0	0	0
GustSpeed	-0.19156	-0.29843	-0.31887	-0.45287		0	0	0	0	0
RH_%	0.038627	0.36783	0.32285	0.3815	-0.35147		0	0	4.4542E-07	0
SolarRad	-0.033802	-0.17505	-0.053074	-0.26591	0.3758	-0.47039		0	6.0971E-11	0
Temp	-0.31787	-0.53324	-0.83958	-0.87902	0.4498	-0.48785	0.29015		0	0
WaterCont	-0.21003	0.061484	-0.44749	-0.39546	0.18888	-0.024704	-0.032005	0.46875		1.1373E-217
WindSpeed	-0.15523	-0.28256	-0.29898	-0.42793	0.95423	-0.35789	0.39268	0.42259	0.15321	

March Pearson's r correlations and p-values.

	C-1	C-4	C-5	C-7	GustSpeed	RH_%	SolarRad	Temp	WaterCont	WindSpeed
C-1		0	4.9407E-324	0	6.2789E-161	0	7.5657E-42	0	0	1.6531E-73
C-4	0.44326		0	0	0	7.8059E-152	1.2168E-143	0	0	0
C-5	0.1807	0.51424		0	0	0	2.2327E-305	0	0	0
C-7	0.436	0.67631	0.61442		0	0	0	0	0	0
GustSpeed	-0.12743	-0.27238	-0.3068	-0.38055		0	0	0	0	0
RH_%	-0.32468	0.12376	0.38539	0.24558	-0.34993		0	0	0.054544	0
SolarRad	-0.064087	-0.12035	-0.17543	-0.35839	0.41121	-0.4366		0	3.9978E-124	0
Temp	-0.30298	-0.6103	-0.78949	-0.86081	0.5111	-0.37995	0.40305		0	0
WaterCont	-0.50883	-0.35685	-0.26161	-0.46495	0.2538	-0.0090994	0.11181	0.44754		0
WindSpeed	-0.085687	-0.24525	-0.30768	-0.36431	0.96012	-0.35033	0.41508	0.49086	0.22257	

April Pearson’s r correlations and p-values.

	C-1	C-4	C-5	C-7	GustSpeed	RH_%	SolarRad	Temp	WaterCont	WindSpeed
C-1		1.8513E-72	4.5057E-09	2.835E-233	0.052125	0	0.020703	3.7978E-94	0	2.5203E-08
C-4	0.086455		0	0	7.5592E-321	0	2.1685E-246	0	0	1.9567E-290
C-5	-0.02821	0.77234		0	0.010731	0	1.0541E-86	0	0	2.6824E-06
C-7	0.15594	0.54942	0.63781		0	0	0	0	9.2497E-233	0
GustSpeed	0.0098717	-0.19283	-0.012968	-0.23102		0	0	0	0.75147	0
RH_%	-0.32596	0.31952	0.2141	0.36888	-0.39204		0	0	4.3804E-29	0
SolarRad	-0.011759	-0.16918	-0.10007	-0.29808	0.42384	-0.52451		0	1.4716E-299	0
Temp	-0.10435	-0.69203	-0.74917	-0.77618	0.3386	-0.50347	0.46817		0	0
WaterCont	-0.29439	-0.31207	-0.4105	-0.16445	-0.0016098	-0.056853	0.18639	0.41771		0.9642
WindSpeed	0.028317	-0.18356	-0.023855	-0.21997	0.95564	-0.37377	0.41431	0.31435	0.00022814	